Translational Stroke Research (2020) 11:267–287
https://doi.org/10.1007/s12975-019-00711-0

ORIGINAL ARTICLE

Activation of Sigma-1 Receptor Enhanced Pericyte Survival via the Interplay Between Apoptosis and Autophagy: Implications for Blood–Brain Barrier Integrity in Stroke

Yuan Zhang[1] · Xiaotian Zhang[2] · Qiangqiang Wei[3] · Shuo Leng[4] · Cai Li[5] · Bing Han[1] · Ying Bai[1] · Huibin Zhang[6] · Honghong Yao[1,7]

Received: 18 January 2019 / Revised: 21 May 2019 / Accepted: 6 June 2019 / Published online: 9 July 2019

Abstract

Stroke is a cerebrovascular disorder that affects many people worldwide. Pericytes play an important role in stroke progression and recovery. The sigma-1 receptor (σ-1R) signaling pathway has been suggested as having promising neuroprotective potential in treating stroke; however, whether σ-1R activation regulates pericyte function remains unknown. The aim of this study was to elucidate the role of σ-1R and a novel σ-1R agonist in pericytes following ischemic stroke. An ischemic stroke animal model was induced by photothrombotic middle cerebral artery occlusion (pMCAO) in σ-1R knockout (KO) and wild-type (WT) mice. After pMCAO, there was significant pericyte loss and coverage in σ-1R KO mice compared with WT mice as determined using transmission electron microscopy, immunofluorescence staining, and western blot. Interestingly, a novel σ-1R agonist decreased infarct volume and blood–brain barrier damage with a concomitant amelioration of pericyte loss, as determined by western blot. Further studies indicated that cell apoptosis and autophagy were induced in an in vivo pMCAO ischemic stroke animal model and an in vitro oxygen glucose deprivation-treatment group. Inhibition of autophagy using a pharmacological approach significantly mitigated pericyte apoptosis, suggesting that autophagy was upstream of apoptosis in pericytes. Both in vivo and in vitro studies indicated that the σ-1R agonist significantly decreased cell apoptosis via inhibition of autophagy with a subsequent enhancement of pericyte survival. This study identified the unique roles for σ-1R in mediating pericyte survival via the regulation of the interplay between apoptosis and autophagy, suggesting that a novel σ-1R agonist may be a promising therapeutic agent for the treatment of stroke patients.

Keywords Stroke · Sigma-1 receptor · Blood–brain barrier · Pericyte · Apoptosis · Autophagy

Yuan Zhang, Xiaotian Zhang, Qiangqiang Wei and Shuo Leng contributed equally to this work.

Electronic supplementary material The online version of this article (https://doi.org/10.1007/s12975-019-00711-0) contains supplementary material, which is available to authorized users.

✉ Yuan Zhang
yuanzhang@seu.edu.cn

✉ Huibin Zhang
zhanghb80@cpu.edu.cn

✉ Honghong Yao
yaohh@seu.edu.cn

[1] Department of Pharmacology, School of Medicine, Southeast University, Nanjing 210009, Jiangsu, China

[2] PerMed Biomedicine Institute, Shanghai 201203, China

[3] Department of Medicinal Chemistry, China Pharmaceutical University, Nanjing 210009, Jiangsu, China

[4] Center of Interventional Radiology and Vascular Surgery, Department of Radiology, Zhongda Hospital, Medical School, Southeast University, Nanjing 210009, Jiangsu, China

[5] Department of Neurology, Rizhao Hospital of Traditional Chinese Medicine, Rizhao 276800, Shandong, China

[6] Center of Drug Discovery, State Key Laboratory of Natural Medicines, China Pharmaceutical University, Nanjing 210009, Jiangsu, China

[7] Institute of Life Sciences, Key Laboratory of Developmental Genes and Human Disease, Southeast University, Nanjing 210096, Jiangsu, China

Introduction

Stroke is a cerebrovascular disorder accompanied by vascular damage including blood–brain barrier (BBB) dysfunction [1] and is the leading cause of long-term disability and death worldwide [2–6]. BBB destruction is a key event in stroke that enhances the cascade of molecular and cellular events including glial activation, neuroinflammation, vascular malformation, and neuronal death [7, 8], making/rendering the BBB an important target to reduce brain damage in stroke. BBB breakdown is a consequence of stroke and exacerbates stroke outcome [9]. Pericytes are an important component of the BBB and are located between the endothelial cells and astrocytes that line the entire microvasculature [10–12]. The role of pericytes in stroke is gaining increasing attention

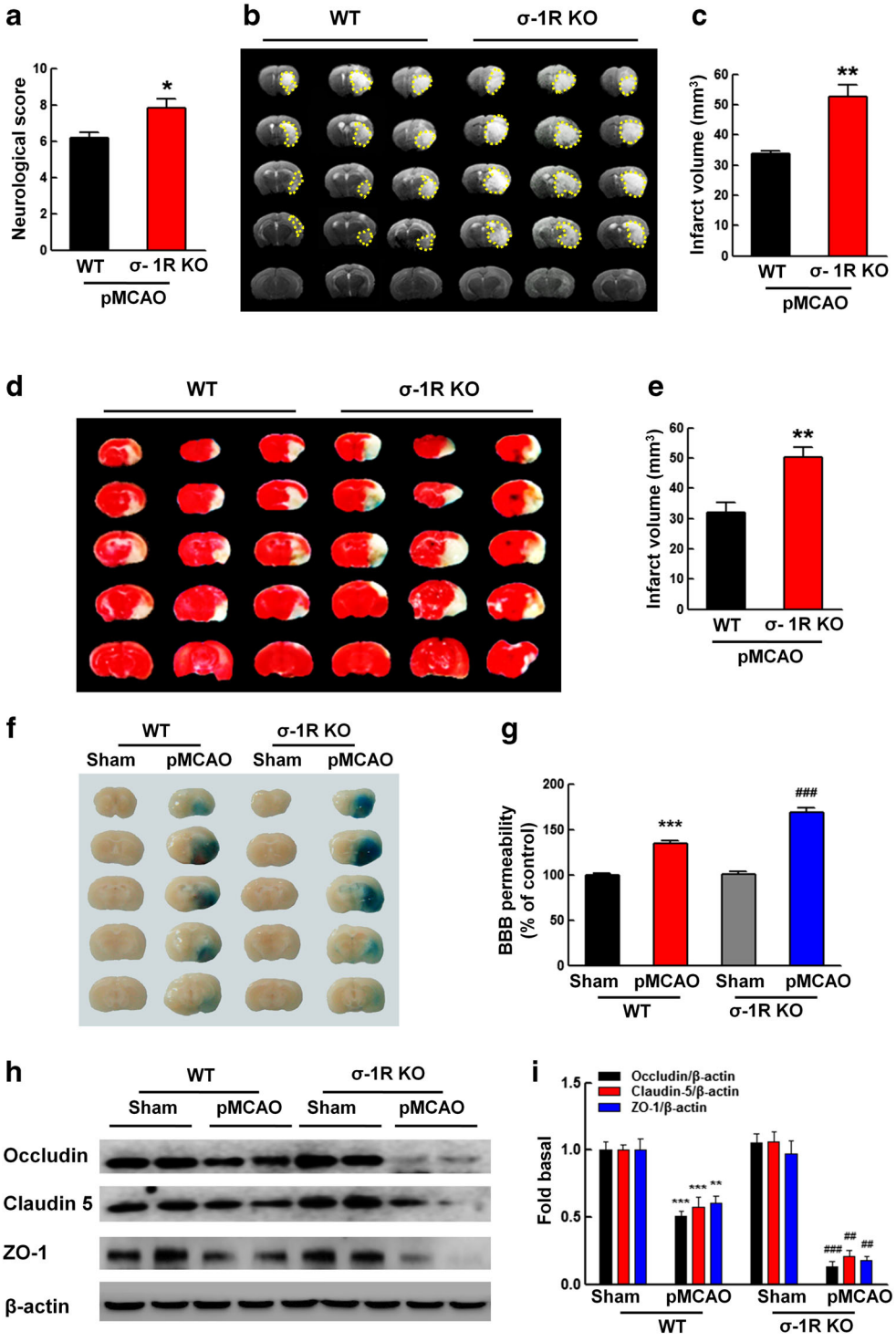

because of the rapid loss of capillary pericytes in experimental animals and humans following cerebral ischemia [13]. Accumulating evidence has indicated that pericyte coverage in blood vessels is important for maintaining BBB integrity [9, 11, 12, 14]. Although the causal relationship of pericyte dysfunction and ischemic stroke is not direct, pericytes may be indirectly involved in the pathogenesis of ischemia via their effects on BBB integrity. However, the molecular mechanisms regulating pericyte function and associated BBB alterations under pathological conditions are still poorly understood. Therefore, novel treatment approaches that may hinder pericyte loss to maintain the integrity of BBB are urgently needed.

Sigma-1 receptor (σ-1R) was initially classified as an opioid receptor; however, further studies indicated that it is a nonopioid receptor that is widely distributed in the central nervous system [15]. As a transmembrane protein, σ-1R primarily resides in the endoplasmic reticulum (ER) and mitochondrial membranes [16] and is highly expressed in neurons and glial cells of brain regions [17]. σ-1R regulates a wide range of processes in the nervous system, including neuritogenesis [18], the communication between ER and mitochondria [17], potassium channel activity [19], the activity of *N*-methyl-D-aspartate [20] and G-protein-coupled receptors [21], calcium homeostasis [17], and microglia activity [22]. Therefore, σ-1R is involved in the pathophysiology of many central and peripheral diseases, such as ischemic stroke [23], Parkinson's disease [24], Alzheimer's disease [25], psychiatric disorders [26], neuroAIDS [27], and pain [28]. A previous study showed that σ-1R activation enhances the intracellular trafficking of brain repair-required biomolecules, following synaptogenesis and brain plasticity enhancement to stimulate recovery after stroke [23]. Additionally, mounting evidence indicates that σ-1R activation provides potent neuroprotection in animal models of ischemic stroke [23, 29, 30]. However, the genetic evidence to elucidate σ-1R roles in the outcomes of stroke is still lacking. Therefore, studies using a genetic approach with the σ-1R knockout (KO) animal model are necessary to further dissect the role of σ-1R in stroke.

Despite intensive research regarding neuroprotective agents designed to block one or more steps of the ischemia cascade, no drugs have been found to yield unequivocal improvements in clinical outcomes [31, 32]. At the clinical level, although no significant effects on functional end points have been observed in the population as a whole [33], a trend of improvement with a selective σ-1R agonist was noted in ischemic stroke patients in a phase II clinic trial [33]. This finding prompted us to further develop novel σ-1R agonists for stroke therapy.

Accumulating evidence indicates that σ-1R activation induces neuronal plasticity and astrocyte membrane raft trafficking activated by hypoxia/aglycemia [23]. Meanwhile, σ-1R activation also affects the migration, motility, phagocytosis, and survival of microglial cells in in vitro ischemia [30, 34, 35]. A recent study identified an unexplored role of σ-1R in alleviating BBB damage via targeting endothelial cells [36]. However, the role of σ-1R on pericytes remains largely unknown. Therefore, our study aimed to investigate the role of σ-1R on BBB damage with an emphasis on pericytes to dissect the role of σ-1R in pericyte function after ischemic stroke.

Fig. 1 Knockdown of σ-1R aggravated cerebral ischemia-induced injury in pMCAO mice. **a** Neurological deficit at 24 h after pMCAO was measured by mNSS. $n = 6$ mice/group. **b** Representative T2-weighted MRI images of WT and σ-1R KO mice 24 h after pMCAO. Infarct volumes were larger in σ-1R KO mice than in WT mice, as demonstrated by MRI. **c** Quantification of T2-weighted MRI images. $n = 4$ animals/group. **d** Brain infarct volume at 24 h after pMCAO was measured on TTC-stained coronal sections. Infarct volumes were larger in σ-1R KO mice than in WT mice at 24 h after pMCAO surgery. **e** Quantification of brain infarct volume. $n = 4$ mice/group. $^{*}p < 0.05$ and $^{**}p < 0.01$ vs. the WT mouse group using Student's *t* test. **f** Representative images of extravasated Evans blue staining of the entire brains of WT and σ-1R KO mice. Knocking down σ-1R aggravated the BBB damage induced by pMCAO. **g** BBB permeability in WT and σ-1R KO mice was determined by measuring the concentrations of brain-extracted Evans blue using spectrophotometry at 620 nm. $n = 4$ mice/group. **h**, **i** The decrease in TJP expression in the ipsilateral side of the brain observed at 24 h after pMCAO surgery was aggravated in σ-1R KO mice. TJP expression levels were determined via western blot analysis (**h**) and quantified through densitometric analysis (**i**). Two representative immunoblots were presented from four mice per group. $^{**}p < 0.01$ and $^{***}p < 0.001$, WT pMCAO vs. WT sham. $^{\#\#}p < 0.01$ and $^{\#\#\#}p < 0.001$, σ-1R KO pMCAO vs. WT pMCAO using one-way ANOVA followed by the Holm–Sidak test

Methods and Materials

Animals

Male C57BL/6J mice, aged 6–8 weeks, were purchased from the Model Animal Research Center of Nanjing University (Nanjing, China). The σ-1R KO mice (null mutant mice, Oprs1−/−) were developed by the Model Animal Research Center of Nanjing University (Nanjing, China). Mouse genotyping was identified by polymerase chain reaction (PCR) with genomic DNA from tail biopsies. The primer sequences used were as follows: (1) 5′-CAACATGGATACCC TTGAGAGATG-3′; and (2) 5′-GCTGGCATGGAACT TGCATAG-3′. The PCR yields only a 756-base pair (bp) product for σ-1R KO mice. Mice were maintained on a 12-h light/dark cycle at 25 °C and provided with free access to commercial rodent chow and tap water before the experiments. The wild-type (WT) mice and the σ-1R KO mice were separately assigned to the sham and stroke groups. All animal surgical procedures were approved by the University Committee on Animal Care of Southeast University.

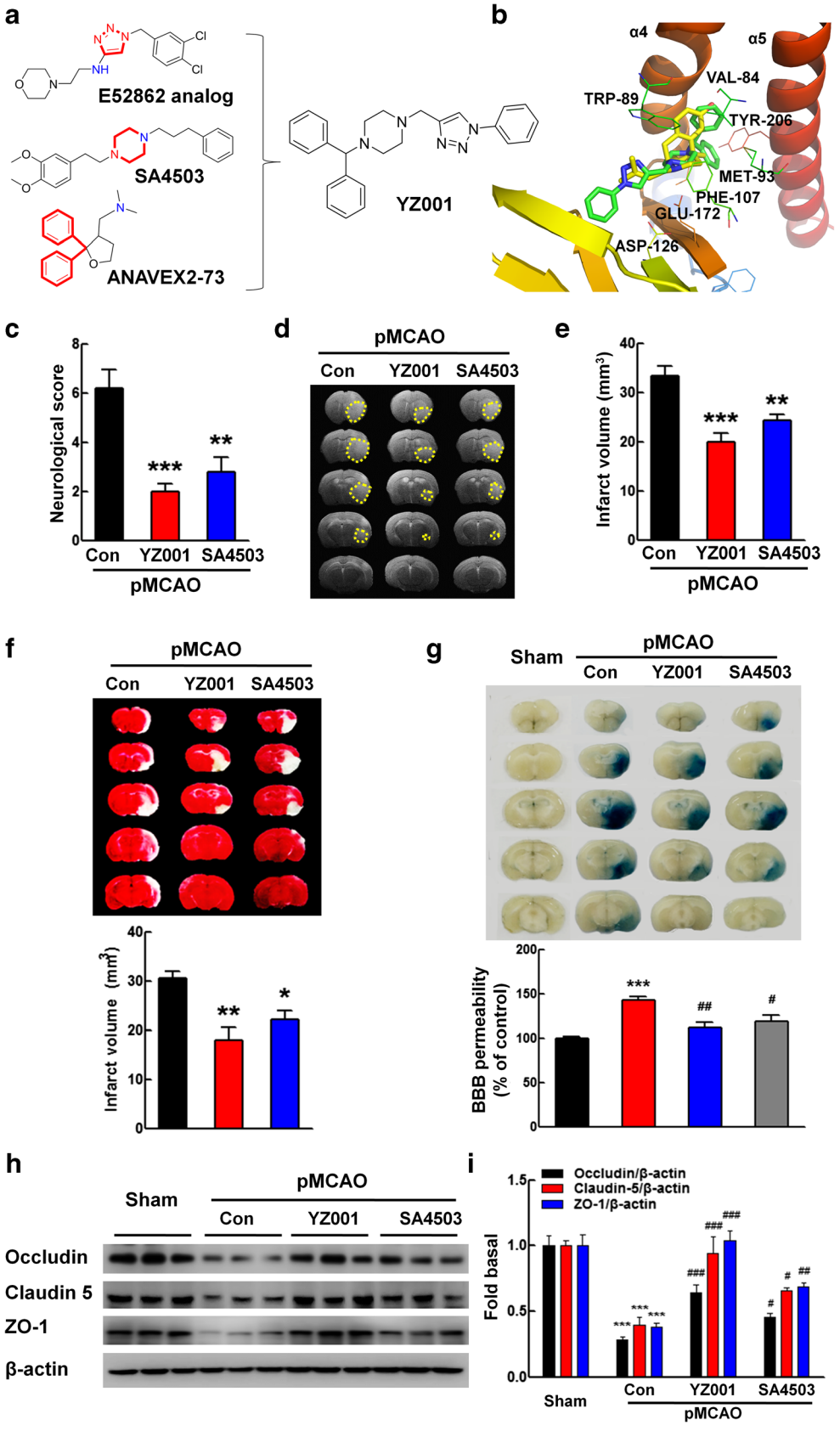
a
E52862 analog
SA4503
ANAVEX2-73
YZ001
b
α4
α5
VAL-84
TRP-89
TYR-206
MET-93
PHE-107
GLU-172
ASP-126
c
Neurological score
Con
YZ001
SA4503
pMCAO
d
pMCAO
Con
YZ001
SA4503
e
Infarct volume (mm3)
Con
YZ001
SA4503
pMCAO
f
pMCAO
Con
YZ001
SA4503
Infarct volume (mm3)
g
Sham
pMCAO
Con
YZ001
SA4503
BBB permeability (% of control)
h
Sham
pMCAO
Con
YZ001
SA4503
Occludin
Claudin 5
ZO-1
β-actin
i
Occludin/β-actin
Claudin-5/β-actin
ZO-1/β-actin
Fold basal
Sham
Con
YZ001
SA4503
pMCAO

◀ **Fig. 2** Compound YZ001 ameliorated cerebral ischemia-induced injury in pMCAO mice. **a** Design strategy for YZ001. **b** The docking conformation of YZ001 with σ-1R. **c** YZ001 pretreatment decreased the high neurological deficit scores induced by pMCAO. YZ001 (0.6 mg/kg) or SA4503 (0.2 mg/kg) was given as pretreatments. Neurological deficit was measured by mNSS at 24 h after pMCAO. $n = 5$ mice/group. **d** Representative T2-weighted MRI images. Infarct volumes demonstrated by MRI were ameliorated in YZ001-pretreated mice. **e** Quantification of T2-weighted MRI images. $n = 4$ mice/group. **f** YZ001 pretreatment decreased the pMCAO-induced increase in infarct volume. Infarct volumes were quantified via TTC staining. $n = 4$ mice/group. $^{*}p < 0.05$, $^{**}p < 0.01$, and $^{***}p < 0.001$ vs. the control group using one-way ANOVA followed by the Holm–Sidak test. **g** Representative images of extravasated Evans blue staining. YZ001 pretreatment ameliorated the BBB damage induced by pMCAO. BBB permeability was determined by measuring the concentrations of brain-extracted Evans blue using spectrophotometry at 620 nm. $n = 4$ mice/group. **h**, **i** YZ001 pretreatment ameliorated the decrease in TJP expression in the ipsilateral side of the brain induced by pMCAO. TJP expression levels were determined via western blot analysis (**h**) and quantified through densitometric analysis (**i**). Three representative immunoblots were presented from six mice per group. $^{***}p < 0.001$ vs. the sham group; $^{\#}p < 0.05$, $^{\#\#}p < 0.01$, and $^{\#\#\#}p < 0.001$ vs. the pMCAO-treated control group using one-way ANOVA followed by the Holm–Sidak test

Design and Synthesis of YZ001

The ligands of σ-1R are diverse in chemical structure, sharing few common features with the exception of a basic nitrogen atom with hydrophobic moieties on both sides: one (the proximal group) lies approximately 2.5 to 3.9 Å away from the basic amine, and the other one (the distal group) is located 6 to 10 Å away (Supplementary Fig. 1A). The positively charged nitrogen of the ligand forms an electrostatic interaction with Glu172 and a cation–π interaction with Phe107, and the rest of the molecule is linearly arranged and fits within the pocket formed by a cluster of hydrophobic residues (Val84, Trp89, Met93, Leu95, Leu105, Ile124, Trp164, and Leu182), completely occluding the interior from the solvent. Notably, the cocrystal structure of σ-1R in complex with small molecule ligands indicates that these ligands occupy different regions of the binding pocket. The primary hydrophobic site of agonists [(+)-pentazocine] points toward helix α4, while antagonists (haloperidol) adopt a more linear pose, with the primary hydrophobic region of the molecule pointing toward the space between helices α4 and α5 (Supplementary Fig. 1B).

Based on scaffold hopping of privileged scaffolds from known bioactive compounds (E-52862 analog, Estever, $Ki\sigma_1 = 61 \pm 20$ nM, $Ki\sigma_2 > 10{,}000$ nM; SA4503, M's Science, $Ki\sigma_1 = 4.34 \pm 0.31$ nM; ANAVEX2-73, Anavex, $Ki\sigma_1 = 860$ nM), our modification strategy was focused on hybridizing three pharmacophoric units to design a new σ-1R agonist YZ001. We selected a diphenyl as the 'anchor' group, which may be crucial for the σ-1R agonist design, and a piperazine ring was introduced to form the key electrostatic interaction with Glu172. Moreover, compared with that observed in (+)-pentazocine or ANAVEX2-73, an extension of the proximal hydrophobic group that occupies the space near the bottom of the β-barrel (near Asp126) may improve σ-1R binding activity (Fig. 2a). To investigate the binding mode of YZ001 to σ-1R, we performed molecular docking experiments in Schrodinger. A comparison of the interactions of (+)-pentazocine and YZ001 bound with σ-1R showed that the positively charged nitrogen of both molecules formed electrostatic interactions with Glu172 and cation–π interactions with Phe107, respectively. In addition, YZ001 was positioned similarly to (+)-pentazocine, and its nonlinear shape forced the diphenyl group to occupy space closer to helix α4 and further from α5 relative to the antagonists (Fig. 2b).

The synthesis of YZ001 is outlined as follows (Supplementary Fig. 2). Aqueous HCl (6 M, 10 ml) was added to a solution of aniline (1.0 g, 11 mmol) at 0 °C, followed by the consecutive dropwise addition of 1 M $NaNO_2$ (10 ml, 10 mmol) in water over a period of 10 min with stirring. After the mixture was stirred for a further 1 h, a solution of NaN_3 (0.84 g, 13 mmol) in H_2O (10 ml) was added to the above reaction mixture with stirring. The reaction mixture was warmed to 25 °C and stirred for 3 h. Then, the solution was poured into H_2O, extracted with EtOAc, dried over Na_2SO_4, filtered, and evaporated to produce a brown liquid (intermediate **1**). Next, a suspension of 1-(diphenylmethyl)-piperazine (0.50 g, 2.0 mmol), K_2CO_3 (0.55 g, 4.0 mmol), and 3-bromoprop-1-yne (0.28 g, 2.4 mmol) in dimethylformamide (DMF; 5 ml) was stirred at ambient temperature for 12 h. Then, the solvent was evaporated, and the product was purified by chromatography on silica (PE:EtOAc = 5:1) to produce a total of 0.31 g white solid (intermediate **2**). Finally, in a round-bottom flask equipped with a mechanical stirrer, intermediate **1** (50 mg, 0.41 mmol) was added, along with intermediate **2** (0.10 g, 0.34 mmol), MeOH (4 ml), $CuSO_4$ pentahydrate (37 mg, 0.14 mmol), sodium ascorbate (24 mg, 0.14 mmol), and H_2O (1 ml). The reaction mixture was stirred at room temperature for 12 h and subsequently extracted with dichloromethane (DCM). The combined organic extracts were washed with water and brine and dried over anhydrous $MgSO_4$, followed by filtration and concentration. The residual crude product was purified by flash chromatography using a gradient mixture of DCM–MeOH to provide the pure compound YZ001. The YZ001 structure was confirmed by MS, IR, ^{1}HNMR, and ^{13}CNMR (Supplementary Table 1). The affinity of YZ001 with σ-1R was determined by the binding affinity assays (Supplementary Fig. 3). The K_i value for YZ001 was 3.926 ± 1.04.

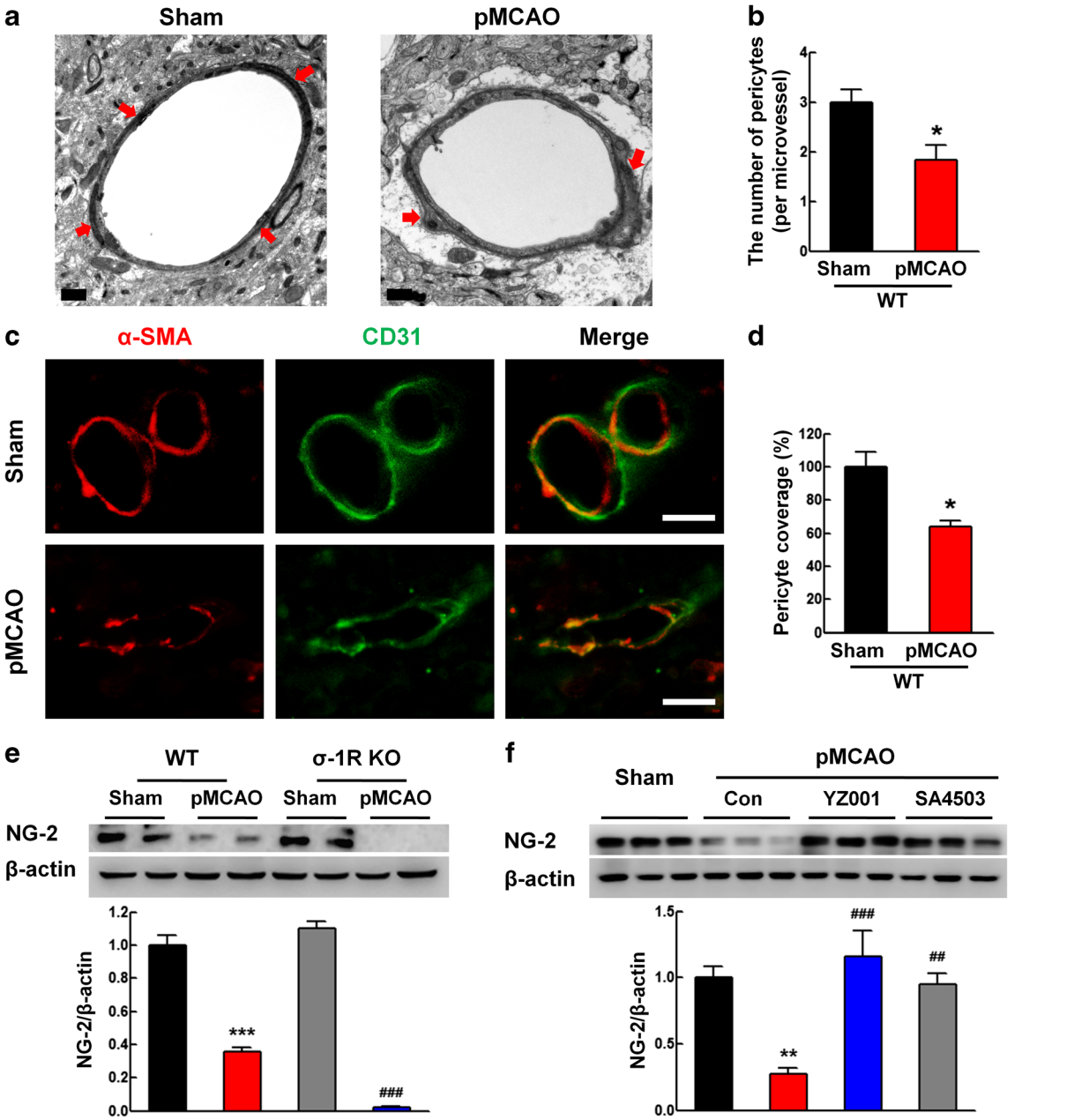

Fig. 3 Compound YZ001 ameliorated the pericyte loss induced by pMCAO. **a** Transmission electron microscopy imaging of brain microvessels showed a reduction in the number of pericytes 24 h after pMCAO. Red arrows indicate the pericytes. Scale bar = 1 μm. **b** Quantification of pericyte numbers in brain microvessels. $n = 4$ mice/group. **c**, **d** Double immunostaining of α-SMA and CD31 in the ipsilateral side of the brain (**c**). The analyzed data (**d**) demonstrated that the microvessels in pMCAO-treated mice exhibited less pericyte coverage than those in the sham group. α-SMA, red; CD31, green. $n = 4$ mice/group. Scale bar = 20 μm. $^{*}p < 0.05$ vs. the sham group using Student's t test. **e** σ-1R knockdown aggravated the pMCAO-induced decrease in pericytes in the ipsilateral side of the brain. Quantification was performed using densitometric analysis of NG-2 expression. Two representative immunoblots were presented from four mice per group. $^{***}p < 0.001$ vs. the WT sham group, $^{\#\#\#}p < 0.001$ vs. the WT pMCAO group using one-way ANOVA followed by the Holm–Sidak test. **f** YZ001 (0.6 mg/kg) pretreatment ameliorated the pMCAO-induced decrease in pericytes in the ipsilateral side of the brain. Three representative immunoblots were presented from six mice per group. $^{**}p < 0.01$ vs. the sham group, $^{\#\#}p < 0.01$ and $^{\#\#\#}p < 0.001$ vs. the pMCAO-treated control group using one-way ANOVA followed by the Holm–Sidak test

Docking Studies

Docking studies were processed with Glide 5.9 in Schrodinger 2013 suite. The σ-1R protein (PDB id: 6DK1) was extracted from the RCSB Protein Data Bank and prepared with default parameters using Maestro protein preparation wizard. Hydrogen atoms were added to the protein structure, and then, the water molecules were

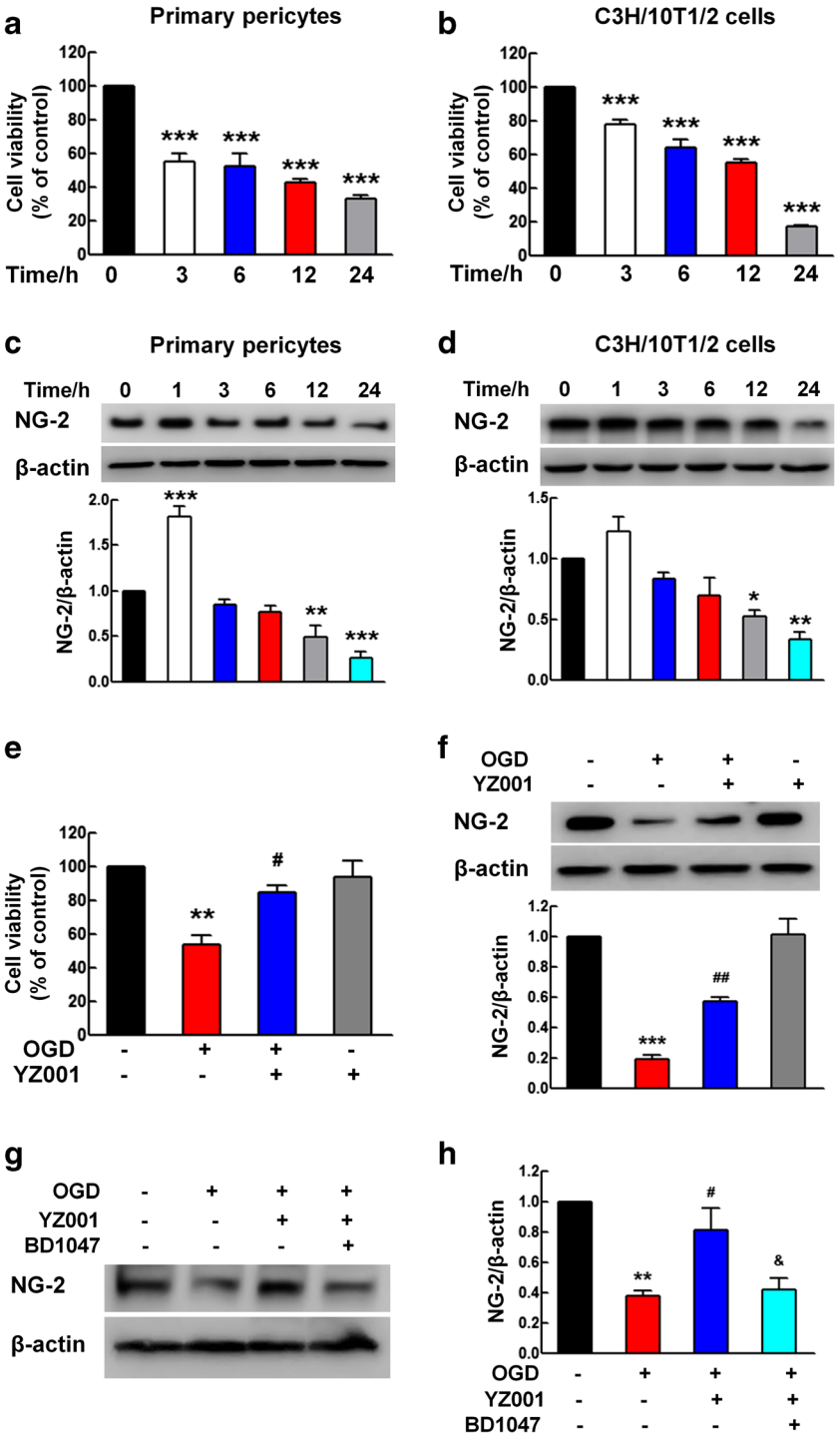

Fig. 4 Compound YZ001 ameliorated the pericyte loss induced by OGD. **a**, **b** OGD decreased the cell viability of primary pericytes (**a**) and C3H/10T1/2 cells (**b**). Cells were subjected to OGD for different durations (3, 6, 12, and 24 h) followed by the MTT assay. **c**, **d** Exposure of primary pericytes (**c**) and C3H/10T1/2 cells (**d**) to OGD for 12 and 24 h attenuated the expression of NG-2. All data are presented as the mean ± SEM of three independent experiments. $^{*}p < 0.05$, $^{**}p < 0.01$, and $^{***}p < 0.001$ vs. the control group using Student's *t* test. **e** YZ001 (10 μM) pretreatment inhibited the OGD-induced decrease in cell viability in primary pericytes. **f** YZ001 pretreatment inhibited the OGD-induced decrease in NG-2 expression in primary pericytes. All data are presented as the mean ± SEM of three independent experiments. $^{**}p < 0.01$ and $^{***}p < 0.001$ vs. the control group, $^{\#}p < 0.05$ and $^{\#\#}p < 0.01$ vs. the OGD-treated control group using one-way ANOVA followed by the Holm–Sidak test. **g**, **h** YZ001 pretreatment prevented the OGD-induced decrease in NG-2 expression, while BD1047 (10 μM) inhibited the protective effect of YZ001 on primary pericytes. NG-2 expression levels were determined via western blot analysis (**g**) and quantified through densitometric analysis (**h**). All data are presented as the mean ± SEM of three independent experiments. $^{**}p < 0.01$ vs. the control group, $^{\#}p < 0.05$ vs. the OGD-treated control group, $^{\&}p < 0.05$ vs. the YZ001-treated OGD group using one-way ANOVA followed by the Holm–Sidak test

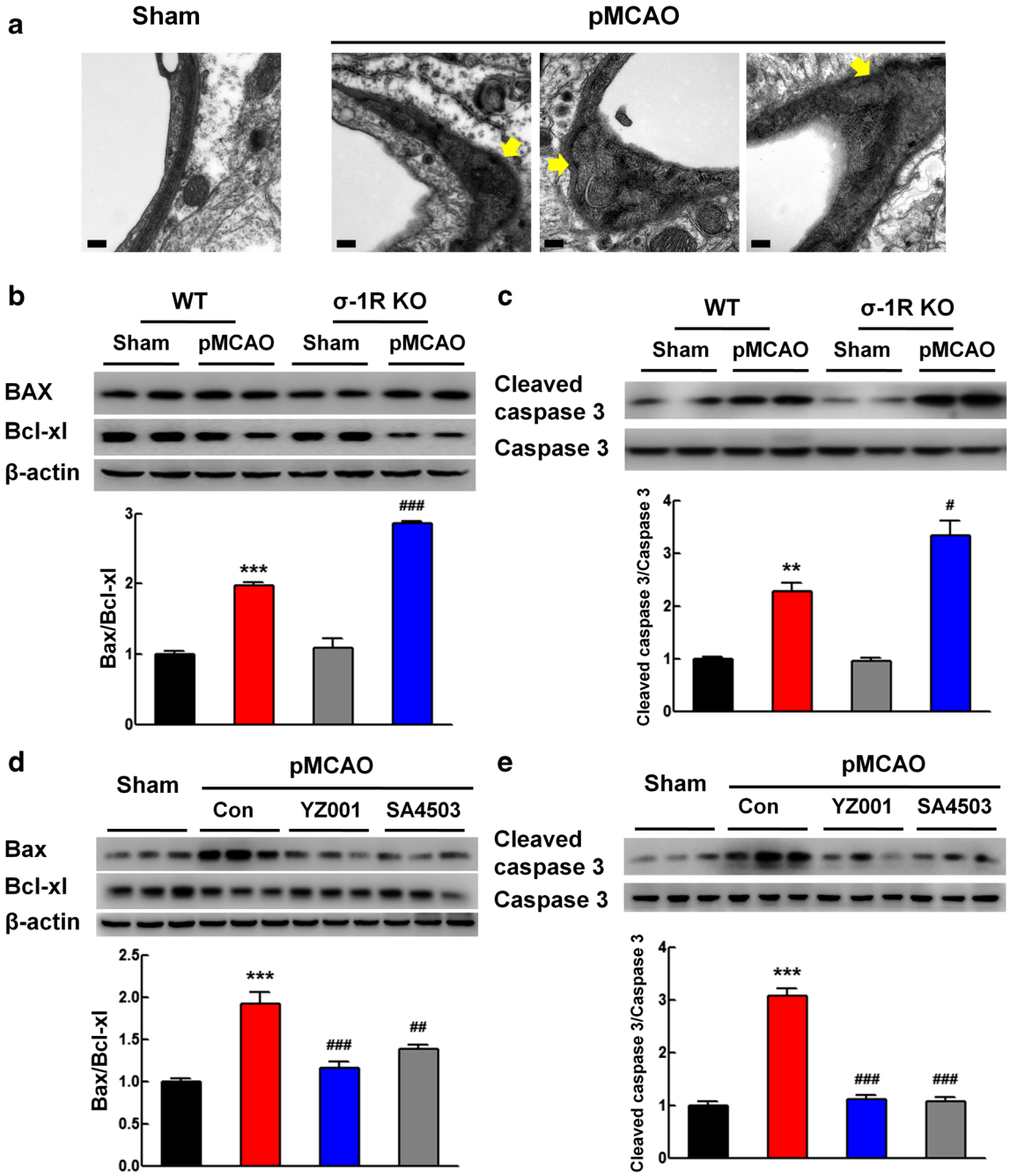

Fig. 5 Compound YZ001 ameliorated the apoptosis of pericytes induced by pMCAO. **a** Transmission electron microscopy imaging of brain microvessels revealed apoptosis (yellow arrows) of pericytes 24 h after pMCAO. $n = 4$ mice/group. **b**, **c** σ-1R knockdown aggravated apoptosis in the pMCAO group. The expression levels of Bax/Bcl-xl (**b**) and cleaved caspase 3/caspase 3 (**c**) were determined via western blot analysis and quantified through densitometric analysis. Two representative immunoblots were presented from four mice per group. $^{*}p < 0.05$ and $^{***}p < 0.001$ vs. the WT sham group, $^{\#}p < 0.05$ and $^{\#\#\#}p < 0.001$ vs. the WT pMCAO group using one-way ANOVA followed by the Holm–Sidak test. **d**, **e** YZ001 (0.6 mg/kg) pretreatment inhibited pMCAO-induced apoptosis in the ipsilateral side of the brain. The expression levels of Bax/Bcl-xl (**d**) and cleaved caspase 3/caspase 3 (**e**) were determined via western blot analysis and quantified through densitometric analysis. Three representative immunoblots were presented from six mice per group. $^{***}p < 0.001$ vs. the sham group, $^{\#\#}p < 0.01$ and $^{\#\#\#}p < 0.001$ vs. the pMCAO-treated control group using one-way ANOVA followed by the Holm–Sidak test

removed. YZ001 was drawn in ChemDraw 2017, optimized using Maestro build panel and saved as an SDF file. Then, a 60-Å box located at the center of the active sites was generated using the grid program to calculate the binding energies between YZ001 and the protein. Firstly, the co-crystallized (+)-pentazocine (PDB id: 6DK1) was redocked into the σ-1R receptor to validate the feasibility of the docking method. Next, molecular docking of YZ001

into the σ-1R complex structure was performed with the standard precision (SP) docking mode. Among all stereoisomers and tautomers of YZ001 that were generated after a number of reasonable evaluations, only one docking conformation was saved. Pymol 1.8.6 was used to analyze the results and draw the 2D figures.

Photothrombotic Middle Cerebral Artery Occlusion

As described in a previous study [37], mice were anesthetized with 1% pentobarbital sodium (i.p., 100 mg/kg) and maintained at 37 ± 1.0 °C on a heating pad during the surgery procedure. To generate stroke, an incision was created between the right orbit and right external auditory canal under a stereoscopic microscope. The scalp and temporalis muscle were exposed, and the zygomatic arch was snipped to expose the proximal section of the right middle cerebral artery (MCA). To effectively occlude the right MCA, a photosensitizer Rose Bengal solution (100 mg/kg, 10 mg/ml, Sigma-Aldrich) was immediately intravenously injected through the tail vein, following a green laser photoillumination (wavelength, 532 nm, GL532TA-100FC, Shanghai Laser & Optics Century) on the MCA for 2 min using an optic fiber (100-μm) connected with a laser diode controller (power at 35, ADR-1805, Shanghai Laser & Optics Century). The sham operation was performed with the same surgical procedures but with phosphate-buffered saline (PBS) injection instead.

Magnetic Resonance Imaging

A 7.0-T small animal magnetic resonance system (Bruker PharmaScan, Ettlingen, Germany) was used to perform magnetic resonance imaging (MRI) as described previously [38]. T2-weighted images were collected in vivo at 24 h after photothrombotic middle cerebral artery occlusion (pMCAO) using a 2D turbo spin-echo sequence (repetition time/echo time = 2000/50 ms). Twelve axial slices (1-mm thickness, 20 × 20 mm field of view, and 256 × 256 matrix) were positioned over the brain, excluding the olfactory bulb. Infarct area analysis was performed by subtracting the area of the nonlesioned ipsilateral hemisphere from that of the contralateral side on T2-weighted images using ImageJ software (National Institutes of Health, Bethesda, MD, USA). Infarct volume was calculated via the integration of infarct areas for all slices of each brain.

Triphenyltetrazolium Chloride Staining

Triphenyltetrazolium chloride (TTC) (Sigma-Aldrich) staining was used to measure infarct volume at 24 h after pMCAO as previously described [37, 38]. Mice were anesthetized with 1% pentobarbital sodium (i.p., 100 mg/kg, Sigma-Aldrich) and perfused with 0.01 M PBS. The brains of the mice were removed immediately and sliced into 1-mm-thick coronal sections with a brain matrix on ice. These brain slices were stained with 1% TTC for 8 min at 37 °C and fixed in 4% paraformaldehyde overnight. The infarct tissues visualized as white were not stained, whereas the viable tissues were stained red. The infarct volume was analyzed using ImageJ software (National Institutes of Health, Bethesda, MD, USA). To correct for brain swelling, infarct area was determined by subtracting the noninfarcted tissue area in the ipsilateral hemisphere from that in the intact contralateral hemisphere. Infarct volume was calculated via the integration of infarct areas for all slices of each brain.

Modified Neurological Severity Score Test

The modified neurological severity score (mNSS) included motor (muscle status, abnormal movement), sensory (visual, tactile, and proprioceptive), and a reflex measure composite score [39]. The scores range from a normal score of 0 to a maximum score of 14, with a higher score indicating more severe neurological injury. Mouse neurological deficits were evaluated at 24 h after pMCAO by an experimenter blinded to the experimental groups.

Evans Blue Extravasation Assay

As described in our previous study [38], 2% Evans blue was injected (4 ml/kg, Sigma-Aldrich) through the tail vein to assess cerebrovascular permeability. After circulation for 4 h, mice were anesthetized with 1% pentobarbital sodium (i.p., 100 mg/kg, Sigma-Aldrich) and perfused with 0.01 M PBS. The brains were then harvested, sliced, and scanned. PBS (1:10 *g*/*v*) and 15% trichloroacetic acid (1:1 *v*/*v*) were used to homogenize and precipitate the brain hemispheres of ischemic and sham mice, followed by centrifugation at 1000×*g* for 10 min. A total of 125 μl of sodium hydroxide (5 M) was added to 500 μl of each supernatant aliquot to adjust the pH value. Evans blue was measured by a spectrophotometer at a wavelength of 620 nm.

Immunofluorescence Staining

Double immunofluorescence staining was performed to evaluate pericyte and microvessel colocalization. Mouse brains encompassing the MCA region were cut into sections (35 μm). After permeabilization with Triton X-100 (0.3% in PBS) for 30 min, the sections were blocked with normal goat serum (NGS, 10% in 0.3% Triton X-100) for 1 h at room temperature. Then, anti-CD31 (ab28364, Abcam) and anti-α-smooth muscle actin (α-SMA;

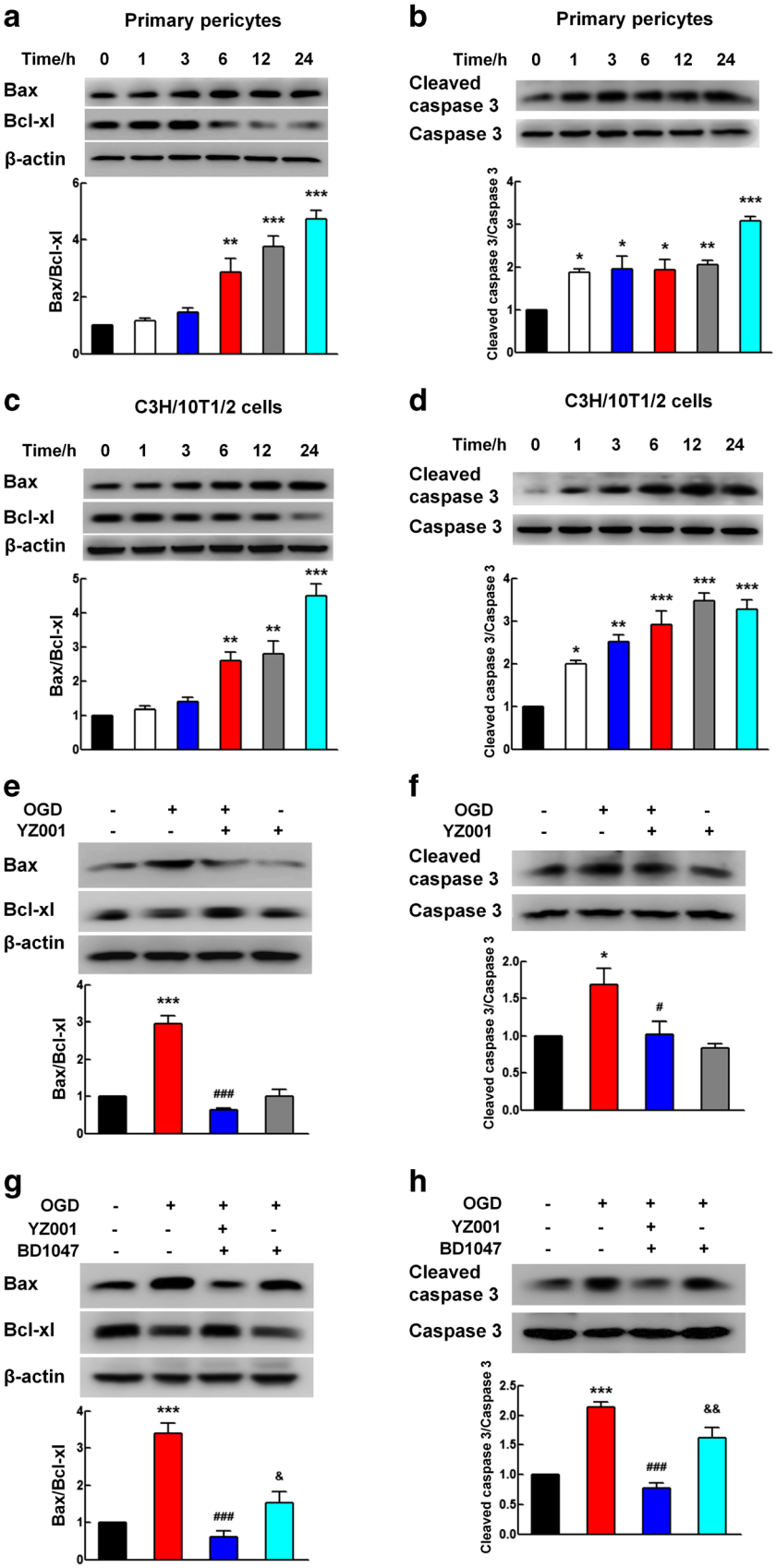
a
Primary pericytes
Time/h 0 1 3 6 12 24
Bax
Bcl-xl
β-actin
Bax/Bcl-xl
b
Primary pericytes
Time/h 0 1 3 6 12 24
Cleaved caspase 3
Caspase 3
Cleaved caspase 3/Caspase 3
c
C3H/10T1/2 cells
Time/h 0 1 3 6 12 24
Bax
Bcl-xl
β-actin
Bax/Bcl-xl
d
C3H/10T1/2 cells
Time/h 0 1 3 6 12 24
Cleaved caspase 3
Caspase 3
Cleaved caspase 3/Caspase 3
e
OGD - + + -
YZ001 - - + +
Bax
Bcl-xl
β-actin
Bax/Bcl-xl
f
OGD - + + -
YZ001 - - + +
Cleaved caspase 3
Caspase 3
Cleaved caspase 3/Caspase 3
g
OGD - + + +
YZ001 - - + -
BD1047 - - + +
Bax
Bcl-xl
β-actin
Bax/Bcl-xl
h
OGD - + + +
YZ001 - - + -
BD1047 - - + +
Cleaved caspase 3
Caspase 3
Cleaved caspase 3/Caspase 3

◀ **Fig. 6** Compound YZ001 ameliorated the apoptosis of pericytes induced by OGD. **a**, **b** Exposure of primary pericytes to OGD increased the expression levels of Bax/Bcl-xl (**a**) and cleaved caspase 3/caspase 3 (**b**). **c**, **d** Exposure of C3H/10T1/2 cells to OGD increased the expression of Bax/Bcl-xl (**c**) and cleaved caspase 3/caspase 3 (**d**). All data are presented as the mean ± SEM of three independent experiments. $^{*}p < 0.05$, $^{**}p < 0.01$, and $^{***}p < 0.001$ vs. the control group using Student's *t* test. **e**, **f** YZ001 (10 μm) pretreatment inhibited the OGD-induced increase in Bax/Bcl-xl (**e**) and cleaved caspase 3/caspase 3 (**f**) in primary pericytes. All data are presented as the mean ± SEM of three independent experiments. $^{*}p < 0.05$ and $^{***}p < 0.001$ vs. the control group, $^{\#}p < 0.05$ and $^{\#\#\#}p < 0.001$ vs. the OGD-treated control group using one-way ANOVA followed by the Holm–Sidak test. **g**, **h** YZ001 pretreatment prevented the OGD-induced increase in Bax/Bcl-xl (**g**) and cleaved caspase 3/caspase 3 (**h**), while BD1047 (10 μM) inhibited the protective effect of YZ001 on primary pericytes. All data are presented as the mean ± SEM of three independent experiments. $^{***}p < 0.001$ vs. the control group, $^{\#\#\#}p < 0.001$ vs. the OGD-treated control group, $^{\&}p < 0.05$ and $^{\&\&}p < 0.01$ vs. the YZ001-treated OGD group using one-way ANOVA followed by the Holm–Sidak test

14395-1-AP, Proteintech) antibodies were incubated with the sections at 4 °C overnight. The next day, the sections were incubated with AlexaFluor 488 (conjugated anti-mouse) and AlexaFluor 594 (conjugated anti-rabbit) IgG (Invitrogen, Grand Island, NY, USA) for 1 h at room temperature and then mounted on poly-L-lysine-coated glass slides.

Transmission Electron Microscopy

Twenty-four hours after pMCAO, mice were anesthetized with 1% pentobarbital sodium (i.p., 100 mg/kg, Sigma-Aldrich) and perfused with 0.01 M PBS followed by PBS containing 4% paraformaldehyde and 0.5% glutaraldehyde. Then, brains were kept overnight in paraformaldehyde and glutaraldehyde (2%, in 0.1 M PBS). The sections of target tissues (50 μm) were collected on a wax block. The sections were postfixed in 1% osmium tetroxide for 1 h, followed by graded ethanol dehydration, and embedded in epoxy resin. Polymerization was performed at 80 °C for 24 h. Ultrathin sections (100 nm) were collected and stained with uranyl acetate and lead citrate. A transmission electron microscope was used for evaluation (Quanta 10, FEI Co.)

Primary Pericyte Culture

The mice were anesthetized with 1% pentobarbital sodium (i.p., 100 mg/kg, Sigma-Aldrich). Then, the brains were extracted and placed in cold PBS. These brains, without the olfactory bulb, cerebellum, and medulla, were thoroughly minced in 10 ml of Eagle's minimum essential medium (EMEM) using a sterilized razor blade and then centrifuged at 1000×*g* for 10 min. Subsequently, the washed tissue was resuspended with EMEM (5 ml). The homogenized cells were mixed with 5 ml of bovine serum albumin (BSA, 25% in PBS). After centrifugation (4000 rpm, 10 min), the lipid layer was removed from the top of the vial. The cell pellet was resuspended in an enzymatic solution containing collagenase (2 mg) and DNAse I (200 μl, 2 μg/ml) in 2 ml of EMEM for 80 min at 37 °C, shaking every 5 min. After the digested brain tissue was mixed with 1.7 volumes of BSA (25% in PBS) followed by centrifugation at 4000 rpm for 10 min, the cell pellet was resuspended in 3 ml of endothelial cell medium (ECM) with fetal bovine serum (FBS, 10%), penicillin/streptomycin (1%), and endothelial cell growth supplement (ECGS, 1%). Then, the cells were plated on coated 6-well plates (0.02% collagen I, Sigma-Aldrich, 2 h, 37 °C). After 20 h, the cells were washed three times with PBS, and the medium was changed to fresh ECM; the medium was then changed every 3 days. After the cells reached confluency, the cultures were harvested with trypsin-EDTA. Cells were kept in ECM for the first two passages. From the third passage, cells were maintained in pericyte medium (ScienCell Research Laboratories, Carlsbad, CA) containing FBS (10%), PS (1%), and PCGS (1%) for the experiments.

Oxygen Glucose Deprivation Treatment

To model ischemia in vitro, primary pericytes and C3H/10T1/2 cells were cultured with glucose-free DMEM (Gibco) in a sealed chamber (MIC-101, Billups-Rothenburg) loaded with mixed gas containing 5% CO_2 and 95% N_2 (25 l/min) for 5 min. The chamber was placed in a water-jacketed incubator (Forma, Thermo Fisher Scientific, Waltham, MA, USA) at 37 °C for different durations indicated in each experiment. The cells in the control group were cultured with normal DMEM (10% FBS) for the same amount of time. The autophagy inhibitor 3-methyladenine (3-MA, 2.5 mM, M9281, Sigma-Aldrich), autophagy inducer rapamycin (1 μM, R0395, Sigma-Aldrich), σ-1R antagonist BD1047 (10 μM, 0956, TOCRIS), and σ-1R agonist PRE084 (3 μM, P2607, Sigma-Aldrich) were dissolved in normal culture medium and added to the cells 1 h before oxygen glucose deprivation (OGD). For OGD, cells were refreshed with glucose-free DMEM (prebalanced in an O_2-free chamber at 37 °C) containing the indicated concentrations of these drugs, and the OGD treatment as described above was immediately started.

MTT Assay

The MTT assay was used to measure pericyte viability. The cells were seeded in 96-well plates for 2 days and exposed to OGD. Cells were incubated with MTT dye (20 μl, 5 mg/ml; Biosharp, BS030C) at 37 °C for 1 h. The medium was aspirated, and the formazan crystals were dissolved by dimethyl sulfoxide (DMSO; 200 μl). The absorbance was obtained by using Synergy H1 Multi-Mode Reader (BioTek, Winooski, VT, USA) at 570 nm wavelength.

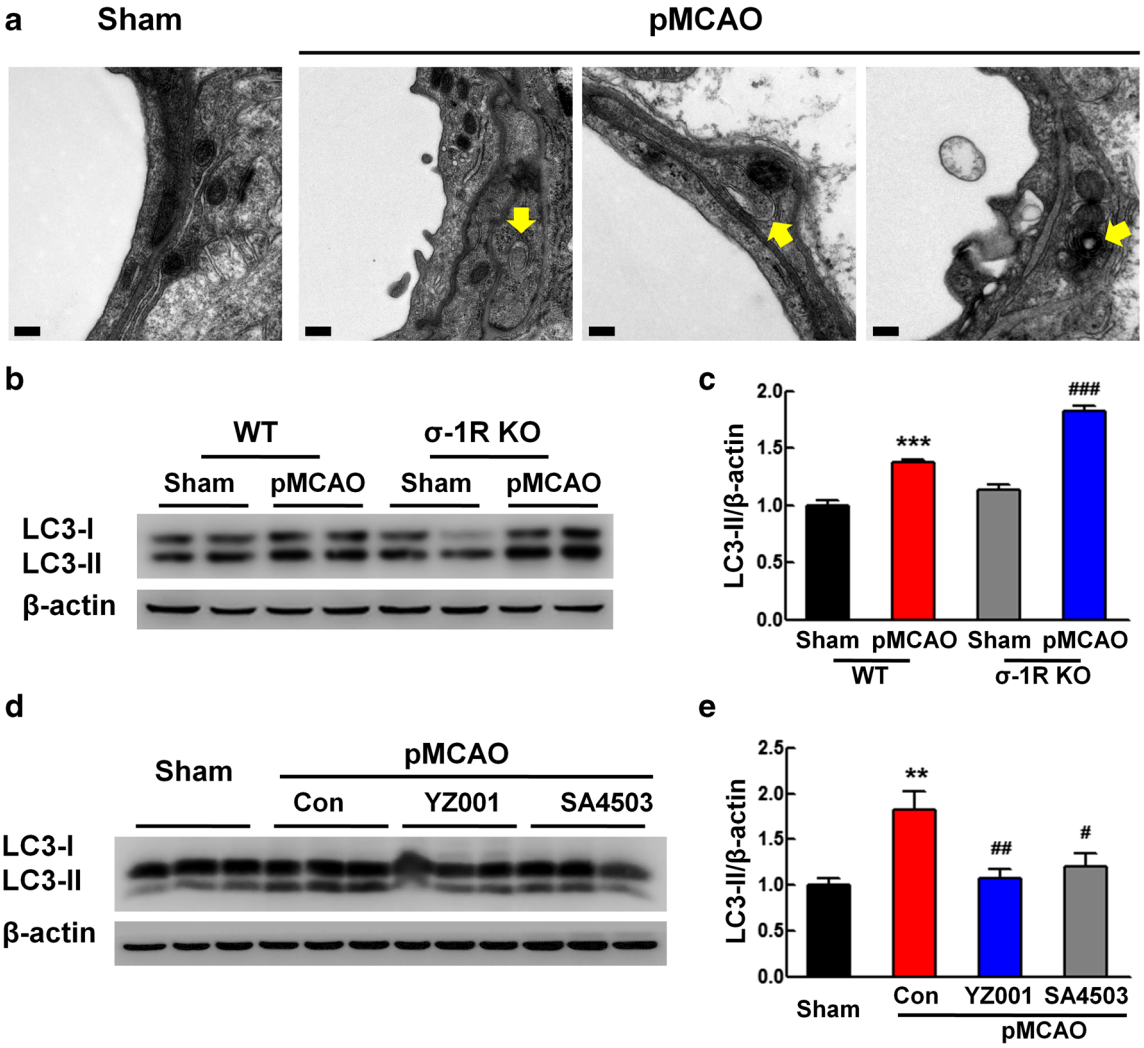

Fig. 7 Compound YZ001 ameliorated the autophagy of pericytes induced by pMCAO. **a** Transmission electron microscopy imaging of brain microvessels showed autolysosomes and double-membraned autophagosomes (yellow arrows) of pericytes 24 h after pMCAO. $n = 4$ mice/group. Scale bar = 0.2 μm. **b**, **c** σ-1R knockdown aggravated autophagy in the pMCAO group. Quantification was performed using densitometric analysis of LC3-II expression. Two representative immunoblots were presented from four mice per group. $^{***}p < 0.001$ vs. the WT sham group, $^{###}p < 0.001$ vs. the WT pMCAO group using one-way ANOVA followed by the Holm–Sidak test. **d**, **e** YZ001 (0.6 mg/kg) pretreatment inhibited pMCAO-induced autophagy in the ipsilateral side of the brain. Quantification was performed using densitometric analysis of LC3-II expression. Three representative immunoblots were presented from six mice per group. $^{***}p < 0.001$ vs. the sham group, $^{###}p < 0.001$ vs. the pMCAO-treated control group using one-way ANOVA followed by the Holm–Sidak test

Western Blot Analysis

The extracted protein (RIPA lysis buffer, Beyotime, P0013B) was separated by 12 or 8% sodium dodecyl sulfate-polyacrylamide gel electrophoresis and electrophoretically transferred onto polyvinylidene fluoride membranes. After blocking with nonfat dry milk (5% in Tris-buffered saline with Tween-20), membranes were probed with antibodies overnight at 4 °C. The next day, horseradish peroxidase-conjugated goat anti-mouse/rabbit IgG secondary antibody (1:2000) was incubated for 1 h at room temperature. The antibodies used were as follows: anti-caspase 3 (19677-1-AP) and anti-occludin (13409-1-AP) from Proteintech; anti-claudin-5 (AF0130) from Affinity Bioscience Inc; anti-neural/glial antigen (NG)-2 (AB5320) from Millipore; anti-Bax (2772S) and anti-Bcl-xl (2764S) from Cell Signaling Technology; anti-microtubule-associated protein light chain 3 (LC3; L7543) from Sigma-Aldrich; anti-zonula occludens (ZO)-1 (402300) from Life Technology; and anti-β-actin (AB39199) from AbSci. MicroChemi 4.2® (DNR, Israel) digital image scanner was used for detection. Band intensity quantification was performed using ImageJ software (National Institutes of Health, Bethesda, MD, USA).

Statistical Analysis

SigmaPlot 11.0 was used to perform the statistical analyses. Data are presented as the mean ± standard error of the mean

(SEM). Student's *t* test was used to compare two groups. For multiple comparisons, one-way analysis of variance (ANOVA) followed by the Holm–Sidak test was used. Two-way ANOVA was used, with the two factors being genotype (wild type or σ-1 KO mice) and treatment (sham or pMCAO). The appropriate tests are indicated in the figure legends. p values < 0.05 were considered statistically significant.

Results

Knockdown of σ-1R Aggravated Cerebral Ischemia-Induced Injury in pMCAO Mice

Previous studies have reported that σ-1R provides neuroprotection in an ischemic stroke animal model [23, 29, 30]. To unravel genetic evidence to elucidate the role of σ-1R in the outcomes of stroke, σ-1R KO and WT mice were subjected to pMCAO. After 24 h, the neurological deficit scores were higher in the σ-1R KO mouse group than in the WT mouse group (Fig. 1a). Then, the infarct sizes were evaluated using MRI to determine the extent of the brain damage within the injury territory of WT mice and σ-1R KO mice. Compared with WT mice, σ-1R KO mice displayed a significantly larger infarct volume (Fig. 1b, c). To further confirm these observations, we determined brain infarct volumes by TTC assay with the same surgery. The ischemic infarct was also found to be significantly larger in the σ-1R KO mouse group with this technique (Fig. 1d, e). To investigate the role of σ-1R in ischemia-induced BBB disruption, we examined Evans blue dye leakage at 24 h post-pMCAO. The disruption of the BBB in the σ-1R mouse group was significantly aggravated compared with that in the WT mouse group (Fig. 1f, g). To test the hypothesis that knockdown of σ-1R expression leads to a reduction in the expression of tight junction proteins (TJPs), we performed western blot analysis for claudin-5, occludin, and ZO-1 using the ipsilateral side of the brain after pMCAO. As expected, the pMCAO-treated WT mice displayed decreased TJP expression, and the change was significantly aggravated in σ-1R mice subjected to pMCAO (Fig. 1h, i). These findings suggested that σ-1R plays an important role in preventing cerebral ischemia-induced injury and BBB disruption.

The Compound YZ001 Ameliorated Cerebral Ischemia-Induced Injury in pMCAO Mice

According to our findings, knockdown of σ-1R aggravated the ischemia damage in an ischemic stroke animal model. Therefore, we designed an σ-1R agonist YZ001 and hypothesized that activation of σ-1R provides potent neuroprotection in ischemic stroke. YZ001 was designed and synthesized, hybridized from three pharmacophoric units from the E-52862 analog, SA4503, and ANAVEX2-73 with subsequent optimization (Fig. 2a). E-52862 and SA4503 have been reported to enhance recovery after acute ischemic stroke in a previous study [33, 40]. ANAVEX2-73 has been shown to activate the σ-1R to stimulate neuromodulation and neuroprotection [41]. The docking conformation of YZ001 with σ-1R is shown in Fig. 2b. YZ001 pretreatment significantly reduced neurological deficit scores in mice compared with the control group at 24 h after pMCAO surgery (Fig. 2c). Then, the infarct sizes were evaluated using MRI to determine the extent of the brain damage. Consistently, pretreatment with YZ001 significantly decreased pMCAO-induced infarct sizes (Fig. 2d, e). To further confirm these observations, we determined brain infarct volumes by TTC assay with the same surgery. The ischemic infarct was also significantly smaller in the YZ001-pretreated mouse group than in the control group (Fig. 2f). To investigate the effect of YZ001 on ischemia-induced BBB disruption, we examined Evans blue dye leakage at 24 h post-pMCAO. The disruption of the BBB induced by pMCAO in the YZ001-pretreated mouse group was significantly ameliorated compared with that in the control group (Fig. 2g). Then, the expression of occludin, claudin-5, and ZO-1 was investigated in the ipsilateral side of the brain after pMCAO. As expected, YZ001 pretreatment significantly inhibited the decrease in TJP expression induced by pMCAO (Fig. 2h, i). Taken together, the findings suggested that YZ001 ameliorated the cerebral ischemia-induced injury by maintaining BBB integrity.

The Compound YZ001 Ameliorated Pericyte Loss Induced by pMCAO

Previous evidence has shown that pericyte-covered blood vessels are important for the maintenance of BBB integrity [9, 11, 12, 14]. The brain microvessel ultrastructure was analyzed in the brains of mice sacrificed at 24 h after pMCAO by transmission electron microscopy. There were significantly fewer pericytes in the pMCAO-treated mouse group than in the sham group (Fig. 3a, b). Then, double immunostaining was used to assess the pericyte coverage around the endothelium using antibodies specific for pericytes (α-SMA, red) and the endothelial cell marker (CD31, green) in the ipsilateral side of the brain. As shown in Fig. 3c, d, pMCAO-treated mice exhibited reduced expression of the pericyte marker α-SMA in the ipsilateral side of the brain, suggesting less pericyte coverage than in the sham group (Fig. 3c, d). In addition, western blot revealed significantly decreased expression of another pericyte marker, NG-2, in the pMCAO-treated group.

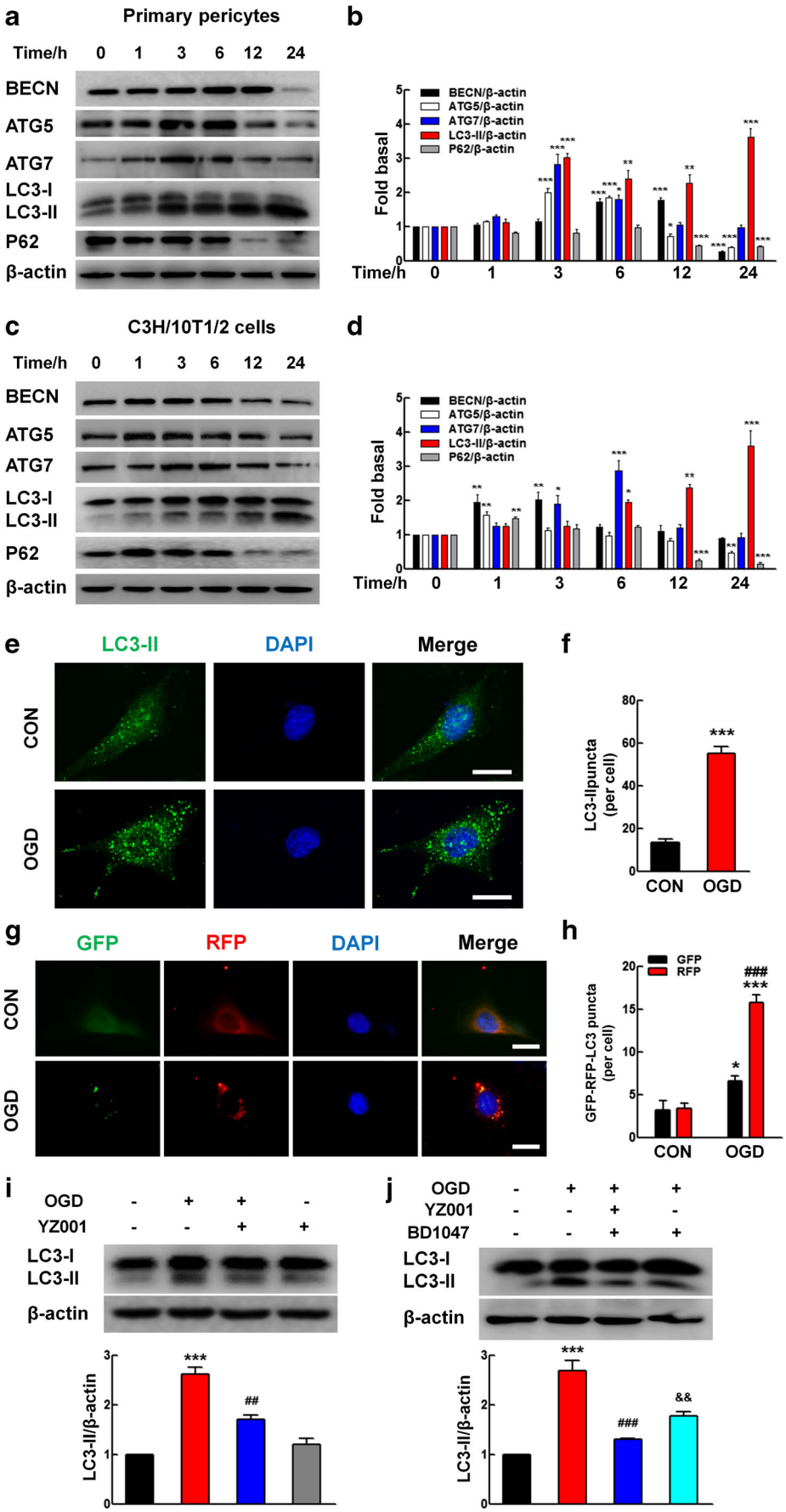
a
Primary pericytes
Time/h 0 1 3 6 12 24
BECN
ATG5
ATG7
LC3-I
LC3-II
P62
β-actin
b
BECN/β-actin
ATG5/β-actin
ATG7/β-actin
LC3-II/β-actin
P62/β-actin
Fold basal
Time/h 0 1 3 6 12 24
c
C3H/10T1/2 cells
Time/h 0 1 3 6 12 24
BECN
ATG5
ATG7
LC3-I
LC3-II
P62
β-actin
d
BECN/β-actin
ATG5/β-actin
ATG7/β-actin
LC3-II/β-actin
P62/β-actin
Fold basal
Time/h 0 1 3 6 12 24
e
LC3-II
DAPI
Merge
CON
OGD
f
LC3-IIpuncta (per cell)
CON OGD
g
GFP
RFP
DAPI
Merge
CON
OGD
h
GFP
RFP
GFP-RFP-LC3 puncta (per cell)
CON OGD
i
OGD - + + -
YZ001 - - + +
LC3-I
LC3-II
β-actin
LC3-II/β-actin
j
OGD - + + +
YZ001 - - + -
BD1047 - - + +
LC3-I
LC3-II
β-actin
LC3-II/β-actin

◀ **Fig. 8** Compound YZ001 ameliorated the autophagy of pericytes induced by OGD. **a**, **b** Exposure of primary pericytes to OGD increased the expression of autophagy proteins and decreased the expression of P62. Quantification was performed using densitometric analysis of BECN, ATG5, ATG7 LC3-II, and P62 expression. **c**, **d** Exposure of C3H/10T1/2 cells to OGD increased the expression of autophagy proteins and decreased the expression of P62. Quantification was performed using densitometric analysis of BECN, ATG5, ATG7 LC3-II, and P62 expression. **e**, **f** Representative immunofluorescence staining of LC3 in C3H/10T1/2 cells. Scale bar = 20 μm. The numbers of LC3 puncta per cell were counted and quantified. All data are presented as the mean ± SEM of three independent experiments. $^{*}p < 0.05$, $^{**}p < 0.01$, and $^{***}p < 0.001$ vs. the control group using Student's *t* test. **g**, **h** C3H/10T1/2 cells were infected with RFP-GFP-LC3 adenovirus and then exposed to OGD for 12 h. The RFP and GFP puncta per cell were counted and quantified. Scale bar = 20 μm. **i** YZ001 (10 μM) pretreatment inhibited the OGD-induced increase in LC3-II expression in primary pericytes. All data are presented as the mean ± SEM of three independent experiments. $^{*}p < 0.05$ and $^{***}p < 0.001$ vs. the control group, $^{\#\#}p < 0.01$ and $^{\#\#\#}p < 0.001$ vs. the OGD-treated control group using one-way ANOVA followed by the Holm–Sidak test. **j** YZ001 pretreatment prevented the OGD-induced increase in LC3-II expression, while BD1047 (10 μM) inhibited the protective effect of YZ001 on primary pericytes. All data are presented as the mean ± SEM of three independent experiments. $^{***}p < 0.001$ vs. the control group, $^{\#\#\#}p < 0.001$ vs. the OGD-treated control group, $^{\&\&}p < 0.01$ vs. the YZ001-treated OGD group using one-way ANOVA followed by the Holm–Sidak test

Nevertheless, these changes were aggravated in the σ-1R KO group (Fig. 3e). Intriguingly, YZ001 ameliorated the pericyte loss induced by pMCAO (Fig. 3f). To further verify the above observations, we subjected primary pericytes (Fig. 4a) and C3H/10T1/2 cells (Fig. 4b) to the ischemia-like insult, OGD. After OGD exposure, cell viability significantly decreased in both primary pericytes and C3H/10T1/2 cells. OGD for 12 and 24 h also decreased the expression of NG-2 in primary pericytes (Fig. 4c) and C3H/10T1/2 cells (Fig. 4d). According to the in vivo findings, σ-1R knockdown seemingly aggravated the pericyte loss induced by pMCAO. Here, we further investigated the role of σ-1R in pericyte survival in vitro. The previously published σ-1R antagonist BD1047 and σ-1R agonist PAE084 were used in primary pericytes and C3H/10T1/2 cells. The σ-1R antagonist BD1047 enhanced the OGD-induced decrease in NG-2 expression in both primary pericytes (Supplementary Fig. 4A) and C3H/10T1/2 cells (Supplementary Fig. 4B). In contrast, the σ-1R agonist PRE084 prevented the pericyte decrease induced by OGD treatment (Supplementary Fig. 4C–D). As expected, YZ001 also inhibited OGD-induced pericyte death in primary pericytes (Fig. 4e, f). Next, further study was undertaken to investigate the effect of the σ-1R antagonist BD1047 on the enhanced pericyte survival induced by YZ001. As shown in Fig. 4g, YZ001 prevented the OGD-induced decrease in NG-2 expression, while BD1047 inhibited the protective effect of YZ001 on pericytes (Fig. 4g). The above findings suggested that YZ001, as an σ-1R agonist, ameliorates cerebral ischemia-induced BBB disruption by preventing pericyte loss.

The Compound YZ001 Ameliorated the Apoptosis of Pericytes Induced by pMCAO

Next, we sought to examine the effect of the compound YZ001 on cell apoptosis in vivo and in vitro. Transmission electron microscopy revealed pericyte apoptosis, in which the nuclei shrank and ruptured (arrow), in pMCAO-treated mice (Fig. 5a). Meanwhile, other indicators of apoptosis, the Bax/Bcl-xl ratio and expression of cleaved caspase 3, were increased in the pMCAO-treated WT group compared to those in the sham WT group. However, knockdown of σ-1R aggravated these changes (Fig. 5b, c). In contrast, YZ001 ameliorated pMCAO-induced pericyte apoptosis (Fig. 5d, e). To verify this observation in vitro, we sought to examine the apoptosis of primary pericytes and C3H/10T1/2 cells. The Bax/Bcl-xl ratio and cleaved caspase 3 expression were markedly increased by OGD in primary pericytes (Fig. 6a, b) and C3H/10T1/2 cells (Fig. 6c, d). Then, we further confirmed the role of σ-1R in pericyte apoptosis. OGD-induced pericyte apoptosis was increased by BD1047 and decreased by PRE084 in both primary pericytes (Supplementary Fig. 5A–D) and C3H/10T1/2 cells (Supplementary Fig. 5E–H). In addition, YZ001 prevented OGD-induced pericyte apoptosis (Fig. 6e, f), and this prevention was inhibited by BD1074 (Fig. 6g, h). These findings suggested that the σ-1R agonist YZ001 prevents pericyte loss by inhibiting pericyte apoptosis.

The Compound YZ001 Ameliorated the Autophagy of Pericytes Induced by pMCAO

Autophagy is also a critical regulatory process of cell survival [42]. Structural analysis via electron microscopy allows for the visualization of autophagy, characterized by the massive accumulation of autophagic vacuoles (autophagosomes) and autolysosomes in the cytoplasm [43]. The accumulation of double-membraned autophagic vacuoles and numerous autolysosomes (arrow) was found in pMCAO-treated mice (Fig. 7a). The expression of LC3-II (autophagy marker) was higher in the pMCAO-treated WT group than in the sham WT group, but this change in LC3-II levels was aggravated in the pMCAO-treated σ-1R KO group (Fig. 7b, c). Moreover, YZ001 ameliorated the autophagy of pericytes induced by pMCAO (Fig. 7d, e). According to the in vivo findings, we hypothesized that autophagy plays another role in regulating the survival of OGD-treated pericytes. We monitored the expression levels of five autophagic markers (Beclin 1 [BECN1], autophagy-related 5 [ATG5], ATG7, LC3-II, and P62) in both primary pericytes and C3H/10T1/2 cells exposed

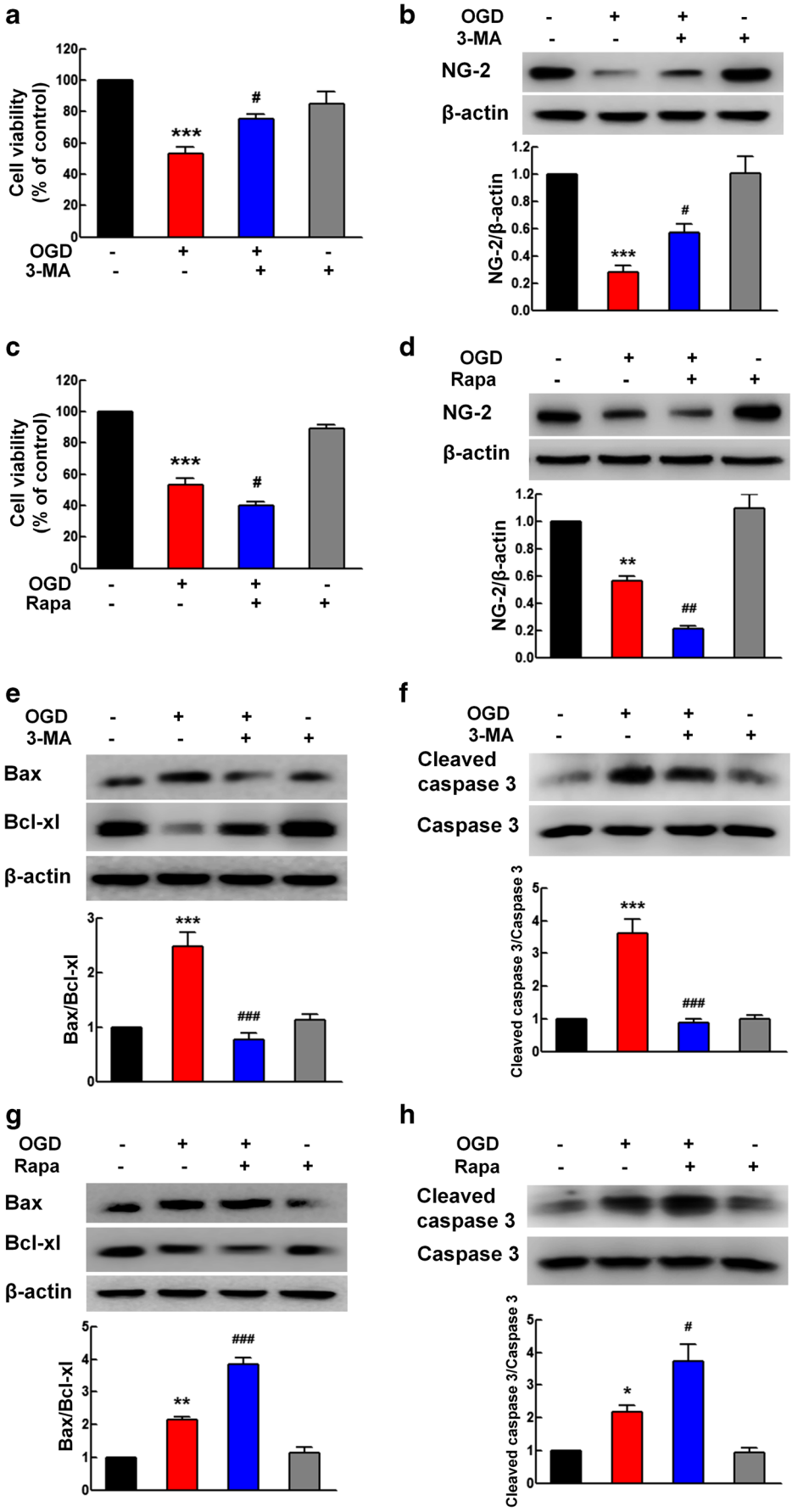
a
Cell viability (% of control)
120
100
80
60
40
20
0
***
#
OGD - + + -
3-MA - - + +
b
OGD - + + -
3-MA - - + +
NG-2
β-actin
NG-2/β-actin
1.2
1.0
0.8
0.6
0.4
0.2
0.0
***
#
c
Cell viability (% of control)
120
100
80
60
40
20
0
***
#
OGD - + + -
Rapa - - + +
d
OGD - + + -
Rapa - - + +
NG-2
β-actin
NG-2/β-actin
1.2
1.0
0.8
0.6
0.4
0.2
0.0
**
##
e
OGD - + + -
3-MA - - + +
Bax
Bcl-xl
β-actin
Bax/Bcl-xl
3
2
1
0
***
###
f
OGD - + + -
3-MA - - + +
Cleaved caspase 3
Caspase 3
Cleaved caspase 3/Caspase 3
5
4
3
2
1
0
***
###
g
OGD - + + -
Rapa - - + +
Bax
Bcl-xl
β-actin
Bax/Bcl-xl
5
4
3
2
1
0
**
###
h
OGD - + + -
Rapa - - + +
Cleaved caspase 3
Caspase 3
Cleaved caspase 3/Caspase 3
5
4
3
2
1
0
*
#

◀ **Fig. 9** Distinct roles of autophagy and apoptosis in OGD-induced pericyte death. **a**, **b** Pretreatment of primary pericytes with the autophagy inhibitor 3-MA (2.5 mM) for 1 h significantly inhibited the OGD-induced decrease in cell viability (**a**) and NG-2 expression (**b**). **c**, **d** Pretreatment with the autophagy inducer rapamycin (1 μM) for 1 h enhanced the OGD-induced decrease in cell viability (**c**) and NG-2 expression (**d**) in primary pericytes. **e**, **f** 3-MA pretreatment inhibited the increase in apoptosis protein expression induced by OGD. The expression levels of Bax/Bcl-xl (**e**) and cleaved caspase 3/caspase 3 (**f**) were determined via western blot analysis and quantified through densitometric analysis. **g**, **h** Rapamycin pretreatment enhanced the effect of OGD in primary pericytes. The expression levels of Bax/Bcl-xl (**g**) and cleaved caspase 3/caspase 3 (**h**) were determined via western blot analysis and quantified through densitometric analysis. All data are presented as the mean ± SEM of three independent experiments. $^{*}p < 0.05$, $^{**}p < 0.01$, and $^{***}p < 0.001$ vs. the control group; $^{\#}p < 0.05$, $^{\#\#}p < 0.01$, and $^{\#\#\#}p < 0.001$ vs. the OGD-treated group using one-way ANOVA followed by the Holm–Sidak test. 3-MA, 3-methyladenine; Rap, rapamycin

to OGD for various durations. As shown in Fig. 8a, b, OGD induced a significant increase in the levels of BECN1, ATG5, ATG7, and LC3-II in primary pericytes. The clearance of P62 is another marker for autophagy. Consistently, P62 expression was downregulated by OGD treatment in primary pericytes (Fig. 8a, b). These findings were further confirmed in C3H/10T1/2 cells (Fig. 8c, d). Furthermore, immunofluorescence staining showed that OGD treatment enhanced the number of vacuoles, as indicated by endogenous LC3-II in C3H/10T1/2 cells (Fig. 8e, f). OGD induced the autophagy of pericytes, which was also confirmed by immunofluorescence staining of C3H/10T1/2 cells transduced with tandem fluorescent-mRFP-GFP-LC3-adenovirus (a specific marker for autophagosome formation). The colocalization of GFP and RFP signals (yellow dots) and RFP-only LC3 dots per cell was significantly increased by OGD treatment in C3H/10T1/2 cells transduced with the autophagosome formation marker (Fig. 8g, h). σ-1R has also been found to play an important role in pericyte autophagy. BD1047 further increased the OGD-induced elevation in LC3-II expression, while PRE084 inhibited this elevation in both primary pericytes (Supplementary Fig. 6A–B) and C3H/10T1/2 cells (Supplementary Fig. 6C–D). Furthermore, YZ001 was found to prevent the autophagy of pericytes induced by OGD treatment (Fig. 8i), while this prevention was inhibited by BD1074 (Fig. 8j). Taken together, these findings suggest that the σ-1R agonist YZ001 inhibited pericyte autophagy to prevent pericyte loss.

Autophagy and Apoptosis Showed Distinct Roles in OGD-Induced Pericyte Loss

To determine the role of autophagy in OGD-induced pericyte loss, we examined whether inhibiting autophagy by 3-MA or inducing autophagy by rapamycin could affect cell survival in both primary pericytes and C3H/10T1/2 cells. First, we found that pretreatment with 3-MA significantly prevented the OGD-induced decrease in cell viability (Fig. 9a) and NG-2 expression (Fig. 9b), while pretreatment with rapamycin enhanced the OGD-induced decrease in cell viability (Fig. 9c) and NG-2 expression in primary pericytes (Fig. 9d). These finding were confirmed in C3H/10T1/2 cells (Supplementary Fig. 7A–D). Next, to further confirm the role of autophagy in OGD-induced apoptosis, cells were treated with 3-MA, which inhibited the Bax/Bcl-xl ratio and cleaved caspase 3 expression in both primary pericytes (Fig. 9e, f) and C3H/10T1/2 cells (Supplementary Fig. 7E–F). Conversely, pretreatment of cells with rapamycin significantly enhanced the Bax/Bcl-xl ratio and cleaved caspase 3 expression in both primary pericytes (Fig. 9g, h) and C3H/10T1/2 cells (Supplementary Fig. 7G–H). The above findings suggested that inhibition of autophagy may decrease the apoptosis of pericytes to prevent pericyte loss.

Discussion

Our study provides new insights into the role of σ-1R in BBB integrity with emphasis on its effects on pericytes via the interplay of apoptosis and autophagy. We first discovered that σ-1R KO mice showed a much worse pericyte loss than WT mice with concomitant increase in infarct volume and BBB damage. Furthermore, we demonstrated that a novel σ-1R agonist, YZ001, alleviated pericyte loss as well as BBB disruption. This process occurred due to the inhibition of pericyte apoptosis via autophagy caused by σ-1R activation (Fig. 10). Therefore, σ-1R may be a potential therapeutic target for treating pericyte survival and provide insights into the development of therapeutic strategies aimed at restoring the BBB breach in stroke patients.

BBB integrity disruption is a common consequence of stroke and contributes to its progression [44]. The BBB includes brain microvascular endothelial cells (BMECs), pericytes, astrocytic endfeet, and neurons. BMECs form the primary barrier of the BBB, with astrocytic endfeet wrapped around them. Pericytes are sandwiched between BMECs and astrocytes and play a vital role in signaling to both cell types to regulate BBB integrity [45–47]. Pericytes support endothelial cell survival and promote normal tight junction development [12]. Ischemic injury causes the detachment of pericytes from the vascular wall, leading to progressive capillary reduction and BBB breakdown [13, 44, 48]. However, the mechanisms of pericyte regulation associated with BBB breakdown under stroke are still poorly understood. Our previous study demonstrated that pericyte-derived vascular endothelial growth factor (VEGF) disrupts BBB integrity in vitro [49]. Regulator of G protein signaling 5 (RGS5) in pericytes negatively regulates pericyte number and endothelial coverage to ensure

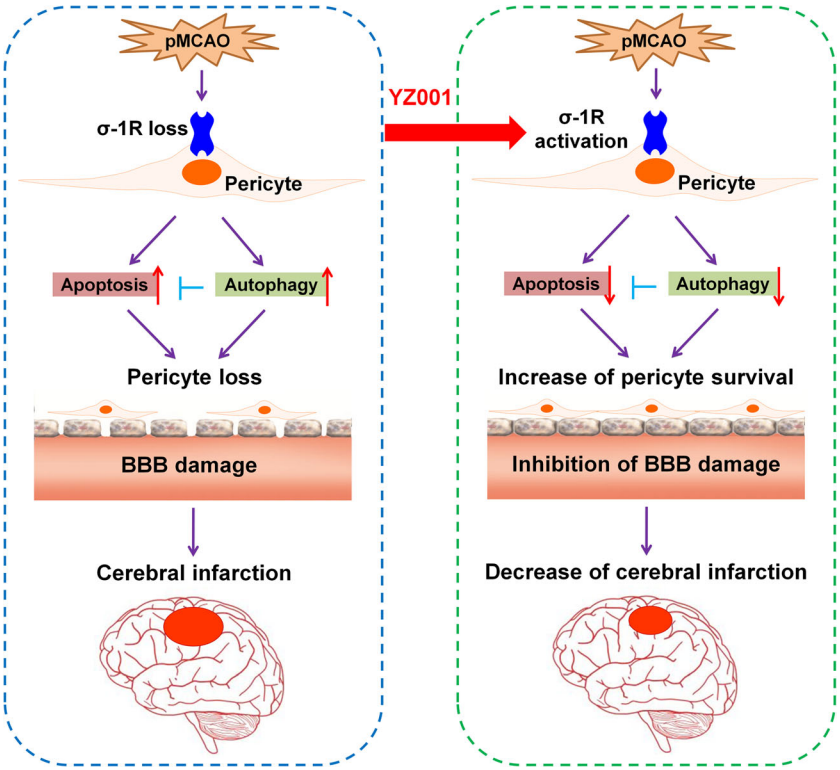

Fig. 10 Inhibition of pericyte apoptosis via autophagy caused by σ-1R activation. σ-1R knockdown induced pericyte loss by increasing the autophagy and apoptosis, which results in BBB disruption and thus contributes to cerebral infarction as demonstrated in the left dashed frame. YZ001 alleviated pericyte loss, which occurred due to the inhibition of pericyte apoptosis via autophagy caused by σ-1R activation, resulting in the inhibition of BBB damage with amelioration of cerebral infarction as demonstrated in the right dashed frame

BBB preservation and neurovascular protection in stroke [50]. Moreover, the inhibition of semaphorin-3e (Sema3E)/plexin-D1 (PlexinD1) signaling increases pericyte recruitment and contributes to functional neovascularization and BBB integrity in stroke [51]. In addition, a recent study indicated that σ-1R activation ameliorates BBB damage in stroke [36]. In this study, the expression of the pericyte marker NG-2 was decreased 24 h after pMCAO, and this reduction was greater in σ-1R KO mice, consistent with previous studies that showed pericyte loss induced by cerebral ischemia in animals and humans [13]. This study is the first to demonstrate that σ-1R regulates pericyte survival, affecting BBB integrity after ischemic stroke.

Mounting evidence suggests a critical role of σ-1R in stroke; therefore, we next sought to develop new drugs targeting σ-1R for the clinical therapy of ischemic stroke. In a phase II clinical trial, the selective σ-1R agonist SA4503 induced a greater improvement in ischemic stroke patients with greater pretreatment deficits [33], although there was no significant difference between the treated and untreated groups. This finding prompted us to develop another novel σ-1R agonist for stroke therapy: the novel σ-1R agonist YZ001, which was designed in this study. Administration of YZ001 significantly ameliorated pericyte loss, infarct volume, and BBB damage. Excitingly, our findings showed that YZ001 treatment exerted a better effect on stroke outcomes than SA4503. Herein, we postulated that alleviation of pericyte loss by YZ001 might contribute to the improvement of stroke outcomes.

Consistent with our findings, different acute brain injury or neurodegeneration experimental models have shown the neuroprotective effect of σ-1R agonists. 4-Phenyl-1-(4-phenylbutyl) piperidine (PPBB) reduced infarct volume in the rat transient MCAO (tMCAO) model by reducing neuronal nitric oxide production without altering dopamine accumulation [52, 53]. Infarct size reduction was also found in rats treated with PRE084 through the enhancement of anti-inflammatory cytokines after stroke in rats [29]. Furthermore, dimemorfan modulated σ-1R-dependent signals, which prevented glutamate accumulation and downstream pathologic events against ischemic stroke in rats [54]. In contrast, the σ-1R antagonist S1RA ameliorated post-stroke neurological deficits and suppressed matrix metalloproteinase (MMP)-9 expression [40]. In the present work, the effects of YZ001 were similar to those of the other evaluated σ-1R agonists, such as PRE084. Meanwhile, BD1047 behaved as an antagonist and blocked the protective effects of YZ001 on pericyte survival. However, in addition to pericytes, YZ001 treatment also ameliorated the cell death of astrocytes and neurons induced by OGD in vitro as well as pMCAO in vivo (Supplementary Figs. 8 and 9), which was consistent with previous findings reporting that σ-1R activation in astrocytes and neurons enhanced brain plasticity and functional recovery after experimental stroke [23].

Autophagy is a fundamentally active process to maintain cellular homeostasis and is necessary for cell survival; however, the role of autophagy in ischemic stroke remains

controversial. Some studies have indicated that autophagy is harmful for neurons in ischemic stroke, and inhibiting autophagy decreases infarct size and augments neurological scores [55, 56]. However, other studies have suggested that the activation or enhancement of autophagy protects against ischemia reperfusion-induced injury [57]. Regarding the role of autophagy in pericyte survival, a previous study revealed a novel mechanism of autophagy disturbance secondary to nitrosative stress-induced tyrosine nitration of transient receptor potential cation channel, subfamily M, member 2 (TRPM2) during pericyte injury [58]. Intriguingly, a dual role for autophagy in diabetic retinopathy has been noted, where autophagy protects cells under mild stress but promotes cell death under more severe stress [59]. Our study revealed that the number of pericytes significantly decreased with a concomitant increase in autophagic pericytes after pMCAO treatment, which is in agreement with the reported activation of autophagic pathways by pericytes to modulate their cell survival in hypoxic and ischemic injuries [60]. In this study, YZ001 treatment in pericytes significantly inhibited cell apoptosis via autophagy both in an in vivo pMCAO stroke model and in vitro OGD-treated pericytes, suggesting that the compound YZ001 may be a new drug candidate for clinical studies as a novel σ-1R agonist.

In conclusion, the novel σ-1R agonist YZ001 decreased infarct volume in pMCAO mice, and this decrease was associated with an amelioration of pericyte loss via the cooperation of apoptosis and autophagy. Although further study is required in other stroke models, YZ001 may be a promising novel therapeutic agent for the treatment of stroke patients.

Funding Information This work was supported by grants from the National Natural Science Foundation of China (Nos. 81761138048, 81673410, and 81603090), Jiangsu Innovation & Entrepreneurship Talent Program, Jiangsu Innovation & Entrepreneurship Team Program, National Key Research and Development Program of China (2017YFA0104303), and the Fundamental Research Funds for the Central Universities (Nos. 2242018K41007, 2242018K41059, 2242019K40133, and 2242019K40125).

Compliance with Ethical Standards

Conflict of Interest The authors declare that they have no conflict of interest.

Ethical Approval All institutional and national guidelines for the care and use of laboratory animals were followed.

References

1. Sandoval KE, Witt KA. Blood-brain barrier tight junction permeability and ischemic stroke. Neurobiol Dis. 2008;32(2):200–19. https://doi.org/10.1016/j.nbd.2008.08.005.
2. Hu X, De Silva TM, Chen J, Faraci FM. Cerebral vascular disease and neurovascular injury in ischemic stroke. Circ Res. 2017;120(3):449–71. https://doi.org/10.1161/CIRCRESAHA.116.308427.
3. Acosta SA, Tajiri N, Hoover J, Kaneko Y, Borlongan CV. Intravenous bone marrow stem cell grafts preferentially migrate to spleen and abrogate chronic inflammation in stroke. Stroke. 2015;46(9):2616–27. https://doi.org/10.1161/STROKEAHA.115.009854.
4. Baltan S, Morrison RS, Murphy SP. Novel protective effects of histone deacetylase inhibition on stroke and white matter ischemic injury. Neurotherapeutics. 2013;10(4):798–807. https://doi.org/10.1007/s13311-013-0201-x.
5. Denorme F, De Meyer SF. The VWF-GPIb axis in ischaemic stroke: lessons from animal models. Thromb Haemost. 2016;116(4):597–604. https://doi.org/10.1160/TH16-01-0036.
6. Vemuganti R. All's well that transcribes well: non-coding RNAs and post-stroke brain damage. Neurochem Int. 2013;63(5):438–49. https://doi.org/10.1016/j.neuint.2013.07.014.
7. del Zoppo GJ, Hallenbeck JM. Advances in the vascular pathophysiology of ischemic stroke. Thromb Res. 2000;98(3):73–81.
8. Turner RJ, Sharp FR. Implications of MMP9 for blood brain barrier disruption and hemorrhagic transformation following ischemic stroke. Front Cell Neurosci. 2016;10:56. https://doi.org/10.3389/fncel.2016.00056.
9. Gautam J, Yao Y. Roles of pericytes in stroke pathogenesis. Cell Transplant. 2018;27:1798–808. https://doi.org/10.1177/0963689718768455.
10. Bell RD, Winkler EA, Sagare AP, Singh I, LaRue B, Deane R, et al. Pericytes control key neurovascular functions and neuronal phenotype in the adult brain and during brain aging. Neuron. 2010;68(3):409–27. https://doi.org/10.1016/j.neuron.2010.09.043.
11. Daneman R, Zhou L, Kebede AA, Barres BA. Pericytes are required for blood-brain barrier integrity during embryogenesis. Nature. 2010;468(7323):562–6. https://doi.org/10.1038/nature09513.
12. Armulik A, Genove G, Mae M, Nisancioglu MH, Wallgard E, Niaudet C, et al. Pericytes regulate the blood-brain barrier. Nature. 2010;468(7323):557–61. https://doi.org/10.1038/nature09522.
13. Fernandez-Klett F, Potas JR, Hilpert D, Blazej K, Radke J, Huck J, et al. Early loss of pericytes and perivascular stromal cell-induced scar formation after stroke. J Cereb Blood Flow Metab. 2013;33(3):428–39. https://doi.org/10.1038/jcbfm.2012.187.
14. Dohgu S, Takata F, Kataoka Y. Brain pericytes regulate the blood-brain barrier function. Nihon Yakurigaku Zasshi. 2015;146(1):63–5. https://doi.org/10.1254/fpj.146.63.
15. Su TP, London ED, Jaffe JH. Steroid binding at sigma receptors suggests a link between endocrine, nervous, and immune systems. Science. 1988;240(4849):219–21.
16. Kourrich S, Su TP, Fujimoto M, Bonci A. The sigma-1 receptor: roles in neuronal plasticity and disease. Trends Neurosci. 2012;35(12):762–71. https://doi.org/10.1016/j.tins.2012.09.007.
17. Hayashi T, Su TP. Sigma-1 receptor chaperones at the ER-mitochondrion interface regulate Ca(2+) signaling and cell survival. Cell. 2007;131(3):596–610. https://doi.org/10.1016/j.cell.2007.08.036.
18. Takebayashi M, Hayashi T, Su TP. Sigma-1 receptors potentiate epidermal growth factor signaling towards neuritogenesis in PC12 cells: potential relation to lipid raft reconstitution. Synapse. 2004;53(2):90–103. https://doi.org/10.1002/syn.20041.
19. Aydar E, Palmer CP, Klyachko VA, Jackson MB. The sigma receptor as a ligand-regulated auxiliary potassium channel subunit. Neuron. 2002;34(3):399–410.
20. Zhang XJ, Liu LL, Jiang SX, Zhong YM, Yang XL. Activation of the zeta receptor 1 suppresses NMDA responses in rat retinal ganglion cells. Neuroscience. 2011;177:12–22. https://doi.org/10.1016/j.neuroscience.2010.12.064.
21. Kim FJ, Kovalyshyn I, Burgman M, Neilan C, Chien CC, Pasternak GW. Sigma 1 receptor modulation of G-protein-coupled receptor

signaling: potentiation of opioid transduction independent from receptor binding. Mol Pharmacol. 2010;77(4):695–703. https://doi.org/10.1124/mol.109.057083.
22. Hall AA, Herrera Y, Ajmo CT Jr, Cuevas J, Pennypacker KR. Sigma receptors suppress multiple aspects of microglial activation. Glia. 2009;57(7):744–54. https://doi.org/10.1002/glia.20802.
23. Ruscher K, Shamloo M, Rickhag M, Ladunga I, Soriano L, Gisselsson L, et al. The sigma-1 receptor enhances brain plasticity and functional recovery after experimental stroke. Brain. 2011;134(Pt 3:732–46. https://doi.org/10.1093/brain/awq367.
24. Francardo V, Bez F, Wieloch T, Nissbrandt H, Ruscher K, Cenci MA. Pharmacological stimulation of sigma-1 receptors has neurorestorative effects in experimental parkinsonism. Brain. 2014;137(Pt 7:1998–2014. https://doi.org/10.1093/brain/awu107.
25. Hedskog L, Pinho CM, Filadi R, Ronnback A, Hertwig L, Wiehager B, et al. Modulation of the endoplasmic reticulum-mitochondria interface in Alzheimer's disease and related models. Proc Natl Acad Sci U S A. 2013;110(19):7916–21. https://doi.org/10.1073/pnas.1300677110.
26. Moriguchi S, Sakagami H, Yabuki Y, Sasaki Y, Izumi H, Zhang C, et al. Stimulation of sigma-1 receptor ameliorates depressive-like behaviors in CaMKIV null mice. Mol Neurobiol. 2015;52(3):1210–22. https://doi.org/10.1007/s12035-014-8923-2.
27. Yao H, Kim K, Duan M, Hayashi T, Guo M, Morgello S, et al. Cocaine hijacks sigma1 receptor to initiate induction of activated leukocyte cell adhesion molecule: implication for increased monocyte adhesion and migration in the CNS. J Neurosci. 2011;31(16):5942–55. https://doi.org/10.1523/JNEUROSCI.5618-10.2011.
28. Tomohisa M, Junpei O, Aki M, Masato H, Mika F, Kazumi Y, et al. Possible involvement of the sigma-1 receptor chaperone in chemotherapeutic-induced neuropathic pain. Synapse. 2015;69(11):526–32. https://doi.org/10.1002/syn.21844.
29. Allahtavakoli M, Jarrott B. Sigma-1 receptor ligand PRE-084 reduced infarct volume, neurological deficits, pro-inflammatory cytokines and enhanced anti-inflammatory cytokines after embolic stroke in rats. Brain Res Bull. 2011;85(3–4):219–24. https://doi.org/10.1016/j.brainresbull.2011.03.019.
30. Ruscher K, Inacio AR, Valind K, Rowshan Ravan A, Kuric E, Wieloch T. Effects of the sigma-1 receptor agonist 1-(3,4-dimethoxyphenethyl)-4-(3-phenylpropyl)-piperazine dihydrochloride on inflammation after stroke. PLoS One. 2012;7(9):e45118. https://doi.org/10.1371/journal.pone.0045118.
31. Fisher M, Schaebitz W. An overview of acute stroke therapy: past, present, and future. Arch Intern Med. 2000;160(21):3196–206.
32. Catanese L, Tarsia J, Fisher M. Acute ischemic stroke therapy overview. Circ Res. 2017;120(3):541–58. https://doi.org/10.1161/CIRCRESAHA.116.309278.
33. Urfer R, Moebius HJ, Skoloudik D, Santamarina E, Sato W, Mita S, et al. Phase II trial of the sigma-1 receptor agonist cutamesine (SA4503) for recovery enhancement after acute ischemic stroke. Stroke. 2014;45(11):3304–10. https://doi.org/10.1161/STROKEAHA.114.005835.
34. Behensky AA, Cortes-Salva M, Seminerio MJ, Matsumoto RR, Antilla JC, Cuevas J. In vitro evaluation of guanidine analogs as sigma receptor ligands for potential anti-stroke therapeutics. J Pharmacol Exp Ther. 2013;344(1):155–66. https://doi.org/10.1124/jpet.112.199513.
35. Cuevas J, Rodriguez A, Behensky A, Katnik C. Afobazole modulates microglial function via activation of both sigma-1 and sigma-2 receptors. J Pharmacol Exp Ther. 2011;339(1):161–72. https://doi.org/10.1124/jpet.111.182816.
36. Liu DY, Chi TY, Ji XF, Liu P, Qi XX, Zhu L, et al. Sigma-1 receptor activation alleviates blood-brain barrier dysfunction in vascular dementia mice. Exp Neurol. 2018;308:90–9. https://doi.org/10.1016/j.expneurol.2018.07.002.
37. Zhang X, Wu F, Jiao Y, Tang T, Yang L, Lu C, et al. An increase of sigma-1 receptor in the penumbra neuron after acute ischemic stroke. J Stroke Cerebrovasc Dis. 2017;26(9):1981–7. https://doi.org/10.1016/j.jstrokecerebrovasdis.2017.06.013.
38. Bai Y, Zhang Y, Han B, Yang L, Chen X, Huang R, et al. Circular RNA DLGAP4 ameliorates ischemic stroke outcomes by targeting miR-143 to regulate endothelial-mesenchymal transition associated with blood-brain barrier integrity. J Neurosci. 2018;38(1):32–50. https://doi.org/10.1523/JNEUROSCI.1348-17.2017.
39. Seyfried D, Han Y, Lu D, Chen J, Bydon A, Chopp M. Improvement in neurological outcome after administration of atorvastatin following experimental intracerebral hemorrhage in rats. J Neurosurg. 2004;101(1):104–7. https://doi.org/10.3171/jns.2004.101.1.0104.
40. Sanchez-Blazquez P, Pozo-Rodrigalvarez A, Merlos M, Garzon J. The sigma-1 receptor antagonist, S1RA, reduces stroke damage, ameliorates post-stroke neurological deficits and suppresses the overexpression of MMP-9. Mol Neurobiol. 2018;55(6):4940–51. https://doi.org/10.1007/s12035-017-0697-x.
41. Goguadze N, Zhuravliova E, Morin D, Mikeladze D, Maurice T. Sigma-1 receptor agonists induce oxidative stress in mitochondria and enhance complex I activity in physiological condition but protect against pathological oxidative stress. Neurotox Res. 2017;35:1–18. https://doi.org/10.1007/s12640-017-9838-2.
42. Rabinowitz JD, White E. Autophagy and metabolism. Science. 2010;330(6009):1344–8. https://doi.org/10.1126/science.1193497.
43. Kroemer G, Galluzzi L, Vandenabeele P, Abrams J, Alnemri ES, Baehrecke EH, et al. Classification of cell death: recommendations of the Nomenclature Committee on Cell Death 2009. Cell Death Differ. 2009;16(1):3–11. https://doi.org/10.1038/cdd.2008.150.
44. Melgar MA, Rafols J, Gloss D, Diaz FG. Postischemic reperfusion: ultrastructural blood-brain barrier and hemodynamic correlative changes in an awake model of transient forebrain ischemia. Neurosurgery. 2005;56(3):571–81.
45. Dohgu S, Takata F, Yamauchi A, Nakagawa S, Egawa T, Naito M, et al. Brain pericytes contribute to the induction and up-regulation of blood-brain barrier functions through transforming growth factor-beta production. Brain Res. 2005;1038(2):208–15. https://doi.org/10.1016/j.brainres.2005.01.027.
46. Nakagawa S, Deli MA, Kawaguchi H, Shimizudani T, Shimono T, Kittel A, et al. A new blood-brain barrier model using primary rat brain endothelial cells, pericytes and astrocytes. Neurochem Int. 2009;54(3–4):253–63. https://doi.org/10.1016/j.neuint.2008.12.002.
47. Takata F, Dohgu S, Yamauchi A, Sumi N, Nakagawa S, Naito M, et al. Inhibition of transforming growth factor-beta production in brain pericytes contributes to cyclosporin A-induced dysfunction of the blood-brain barrier. Cell Mol Neurobiol. 2007;27(3):317–28. https://doi.org/10.1007/s10571-006-9125-x.
48. Hall CN, Reynell C, Gesslein B, Hamilton NB, Mishra A, Sutherland BA, et al. Capillary pericytes regulate cerebral blood flow in health and disease. Nature. 2014;508(7494):55–60. https://doi.org/10.1038/nature13165.
49. Bai Y, Zhu X, Chao J, Zhang Y, Qian C, Li P, et al. Pericytes contribute to the disruption of the cerebral endothelial barrier via increasing VEGF expression: implications for stroke. PLoS One. 2015;10(4):e0124362. https://doi.org/10.1371/journal.pone.0124362.
50. Özen I, Roth M, Barbariga M, Gaceb A, Deierborg T, Genové G, et al. Loss of regulator of G-protein signaling 5 leads to neurovascular protection in stroke. Stroke. 2018;49(9):2182–90. https://doi.org/10.1161/STROKEAHA.118.020124.
51. Zhou YF, Li PC, Wu JH, Haslam JA, Mao L, Xia YP, et al. Sema3E/PlexinD1 inhibition is a therapeutic strategy for improving cerebral perfusion and restoring functional loss after stroke in aged

rats. Neurobiol Aging. 2018;70:102–16. https://doi.org/10.1016/j.neurobiolaging.2018.06.003.

52. Goyagi T, Goto S, Bhardwaj A, Dawson VL, Hurn PD, Kirsch JR. Neuroprotective effect of sigma(1)-receptor ligand 4-phenyl-1-(4-phenylbutyl) piperidine (PPBP) is linked to reduced neuronal nitric oxide production. Stroke. 2001;32(7):1613–20.
53. Goyagi T, Bhardwaj A, Koehler RC, Traystman RJ, Hurn PD, Kirsch JR. Potent sigma 1-receptor ligand 4-phenyl-1-(4-phenylbutyl) piperidine provides ischemic neuroprotection without altering dopamine accumulation in vivo in rats. Anesth Analg. 2003;96(2):532–8 table of contents.
54. Shen YC, Wang YH, Chou YC, Liou KT, Yen JC, Wang WY, et al. Dimemorfan protects rats against ischemic stroke through activation of sigma-1 receptor-mediated mechanisms by decreasing glutamate accumulation. J Neurochem. 2008;104(2):558–72. https://doi.org/10.1111/j.1471-4159.2007.05058.x.
55. Wu Z, Zou Z, Zou R, Zhou X, Cui S. Electroacupuncture pretreatment induces tolerance against cerebral ischemia/reperfusion injury through inhibition of the autophagy pathway. Mol Med Rep. 2015;11(6):4438–46. https://doi.org/10.3892/mmr.2015.3253.
56. Dong F, Yao R, Yu H, Liu Y. Neuroprotection of Ro25-6981 against ischemia/reperfusion-induced brain injury via inhibition of autophagy. Cell Mol Neurobiol. 2017;37(4):743–52. https://doi.org/10.1007/s10571-016-0409-5.
57. Zhang X, Yuan Y, Jiang L, Zhang J, Gao J, Shen Z, et al. Endoplasmic reticulum stress induced by tunicamycin and thapsigargin protects against transient ischemic brain injury: involvement of PARK2-dependent mitophagy. Autophagy. 2014;10(10):1801–13. https://doi.org/10.4161/auto.32136.
58. Jiang Q, Gao Y, Wang C, Tao R, Wu Y, Zhan K, et al. Nitration of TRPM2 as a molecular switch induces autophagy during brain pericyte injury. Antioxid Redox Signal. 2017;27(16):1297–316. https://doi.org/10.1089/ars.2016.6873.
59. Fu D, Yu JY, Yang S, Wu M, Hammad SM, Connell AR, et al. Survival or death: a dual role for autophagy in stress-induced pericyte loss in diabetic retinopathy. Diabetologia. 2016;59(10):2251–61. https://doi.org/10.1007/s00125-016-4058-5.
60. Engelhardt S, Huang SF, Patkar S, Gassmann M, Ogunshola OO. Differential responses of blood-brain barrier associated cells to hypoxia and ischemia: a comparative study. Fluids Barriers CNS. 2015;12:4. https://doi.org/10.1186/2045-8118-12-4.